Impacts of strong wind events on sea ice and water mass properties in Antarctic coastal polynyas

Xiaoqiao Wang[1] · Zhaoru Zhang[1] · Xuezhu Wang[2] · Timo Vihma[3] · Meng Zhou[1] · Lejiang Yu[4] · Petteri Uotila[5] · Dmitry V. Sein[6,7]

Abstract

Strong offshore wind events (SOWEs) occur frequently near the Antarctic coast during austral winter. These wind events are typically associated with passage of synoptic- or meso-scale cyclones, which interact with the katabatic wind field and affect sea ice and oceanic processes in coastal polynyas. Based on numerical simulations from the coupled Finite Element Sea-ice Ocean Model (FESOM) driven by the CORE-II forcing, two coastal polynyas along the East Antarctica coast—the Prydz Bay Polynya and the Shackleton Polynya are selected to examine the response of sea ice and oceanic properties to SOWEs. In these polynyas, the southern or western flanks of cyclones play a crucial role in increasing the offshore winds depending on the local topography. Case studies for both polynyas show that during SOWEs, when the wind speed is 2–3 times higher than normal values, the offshore component of sea ice velocity can increase by 3–4 times. Sea ice concentration can decrease by 20–40%, and sea ice production can increase up to two to four folds. SOWEs increase surface salinity variability and mixed layer depth, and such effects may persist for 5–10 days. Formation of high salinity shelf water (HSSW) is detected in the coastal regions from surface to 800 m after 10–15 days of the SOWEs, while the HSSW features in deep layers exhibit weak response on the synoptic time scale. HSSW formation averaged over winter is notably greater in years with longer duration of SOWEs.

Keywords Antarctic · Strong offshore wind events · Coastal polynyas · Sea ice · High salinity shelf water

✉ Zhaoru Zhang
zrzhang@sjtu.edu.cn

1 School of Oceanography, Shanghai Jiao Tong University, Shanghai, China

2 College of Oceanography, Hohai University, Nanjing, China

3 Meteorological Research, Finnish Meteorological Institute, Helsinki, Finland

4 State Oceanic Administration Key Laboratory for Polar Science, Polar Research Institute of China, Shanghai, China

5 Institute for Atmospheric and Earth System Research/Physics, Faculty of Science, University of Helsinki, Helsinki, Finland

6 Alfred Wegener Institute, Helmholtz Centre for Polar and Marine Research, Bremerhaven, Germany

7 Shirshov Institute of Oceanology, Russian Academy of Sciences, Moscow, Russia

1 Introduction

Around the Antarctic continent, areas with no or little sea ice cover along the coastlines can be observed even during winter. These open water areas surrounded by sea ice are Antarctic coastal polynyas, generally driven by offshore katabatic and synoptic winds (Bromwich et al. 1998; Massom et al. 1998). The new sea ice production within coastal polynyas and the associated brine rejection result in the formation of high salinity shelf water (HSSW), which is a critical source water mass for Antarctic Bottom Water (AABW), a key component of the lower cell of the meridional overturning circulation (Comiso and Gordon 1998; Ohshima et al. 2013; Whitworth et al. 2013).Furthermore, Antarctic coastal polynyas are regarded as important atmospheric CO_2 sink areas (Arrigo et al. 2008; Hoppema and Anderson 2007; Tortell et al. 2012) resulting from deep convection and massive phytoplankton accumulation compared with adjacent waters (Tremblay and Smith 2007), and consequently play a noticeable role in the global climate system.

Numerical studies indicate that the air-sea heat fluxes and sea ice production within the coastal polynyas significantly increase with the strength of katabatic winds (Petrelli et al. 2008; Stössel et al. 2011; Zhang et al. 2015). Mathiot et al. (2010) illustrated that when the katabatic wind speed increases by 15%, the sea ice freezing rate increases by 42%, and the HSSW output increases by 60%. Barthélemy et al. (2012) employed a bias correction for katabatic winds, which compensated for the underestimation of these winds in coarse-resolution global coupled climate model, and such correction enhanced the ice production along the Antarctic coast by up to 50% and the AABW production by up to 2.8 Sv. Most of the earlier studies were focused on the role of wind in Antarctic coastal polynyas on seasonal or longer time scale. However, the coastal winds of Antarctica are actually characterized by high-frequency wind events that are often associated with the passage of synoptic- and meso-scale cyclones (Turner et al. 2009; Weber et al. 2016), and the offshore winds could either be enhanced or weakened during these events depending on the relative location of the coast and the cyclones. We argue that these wind events significantly impact the sea-ice formation and oceanic properties of Antarctic coastal polynyas.

Some recent studies focus on the influence of synoptic-scale wind forcing on sea ice properties in Antarctic coastal polynyas based on satellite observations. Dale et al. (2017) found that sea ice concentration and sea ice motion derived from satellite SSM/I brightness temperatures had large anomalies during a strong wind event in the Ross Sea polynya and strong negative correlations were found between sea ice concentration and wind speed. Cheng et al. (2019) estimated the sea ice production from passive microwave sea ice concentration images based on a thermodynamic model and illustrated that about 68% variation of sea ice production is associated with the wind variation. Studies based on satellite data provide important insights into the response of polynyas to changes in atmospheric forcing, but they also have a few limitations. First, the response of oceanic processes, including convection and the formation of HSSW that directly impact the thermohaline circulation cannot be revealed. Second, in terms of the sea-ice properties, the ice production rate is normally estimated by a combination of satellite-retrieved ice thickness and heat fluxes between the atmosphere and sea ice (Nihashi and Ohshima 2015; Tamura et al. 2016), while sea-ice-ocean heat fluxes are ignored. Haid and Timmermann (2013) concluded that the oceanic heat flux is a non-negligible component of surface heat budget especially at high latitudes, and about 10–20% of the atmospheric heat flux was compensated by the oceanic heat content in sea ice production process. In addition, due to the surrounding sea ice cover and severe wind conditions, very few in-situ measurements can be conducted in Antarctic coastal polynyas in austral winter when HSSW is mainly

produced. In such a situation, ocean-sea-ice models combined with observations become an indispensable method to investigate the response of sea ice and oceanic processes in Antarctic polynya areas to atmospheric forcing.

In this study, a global eddy-resolving ocean-sea-ice model based on the Finite Element Sea-ice Ocean Model (FESOM) is employed to investigate the impacts of strong offshore wind events (SOWEs) on sea ice and water mass formation in two Antarctic coastal polynyas. The main objective of this study is to quantify the sea ice and ocean variability in the polynyas associated with the SOWEs; the response time of different variables is also investigated. The manuscript is organized as follows. Section 2 provides information on the observational data, the numerical model, the model validation results and the analysis methods. Section 3 presents the impacts of SOWEs on the variations of various sea ice and oceanic variables. Discussions on the relationship between sea ice properties and SOWEs and between the HSSW characteristics and SOWEs are given in Sect. 4. Section 5 provides the summary and conclusions.

2 Data and methods

2.1 Model data description

This study utilizes numerical simulations from the global FESOM model version 1.4 (Wang et al. 2014), which combines a hydrostatic primitive-equation ocean model with a dynamic-thermodynamic sea-ice component based on an elastic-viscous-plastic (EVP) solver following Hunke and Dukowicz (1997) and Danilov et al. (2015). The model applies sea surface salinity (SSS) restoring in order to maintain the stability of the finite element calculation (Griffies et al. 2009) and to prevent the model simulation drifting towards unrealistic conditions. This model has varying spatial resolution depending on the local baroclinic Rossby radius and sea surface height variability for most areas (Sein et al. 2016). In the Southern Hemisphere, the model resolution is capped at 7 km along the Antarctic coast. The model has 47 unevenly spaced vertical levels with increasing layer thickness from 10 m at the surface to about 500 m in the deepest layers (Sein et al. 2017). Several bottom topography datasets are used in this FESOM version, including the General Bathymetric Chart of the Oceans (GEBCO), which provides the bottom topography south of 64°N and the International Bathymetric Chart of the Arctic Oceans (IBCAO) north of 69°N. The topography between 64° N and 69° N is assembled as a linear combination of these two datasets (Wang et al. 2014). Furthermore, the one-minute Refined Topography (Rtopo-1) dataset (Timmermann et al. 2010) is used to create the ocean bottom topography, surface elevation of the Antarctic ice sheet/ice shelf system and ice shelf

grounding line in the ice cavity regions around Antarctica (Wang et al. 2014). The ocean is initialized with the temperature and salinity fields from the PHC3.0 global ocean climatology (Steele et al. 2001), and the sea ice model starts with long-term mean sea ice concentration and thickness from the final model state in a spin-up simulation from 1948 to 1988. The 6-hourly atmospheric reanalysis data from the Coordinated Ocean-ice Reference Experiments-Phase II (CORE-II) (Large and Yeager 2009), which are derived from the NCEP/NCAR Reanalysis (Kalnay et al. 1996), are used to drive the FESOM model; the spatial resolution of CORE-II is nominal 1°. The detailed FESOM model configuration and performance with FESOM-XR mesh can be found in Sein et al. (2017). The FESOM simulation spans from 1988 to 2008, and the model results are output as 5-day-average values, which allows us to investigate the response of Antarctic coastal polynyas to atmospheric events on the synoptic scale. The 6-hourly CORE-II forcing data are also processed into 5-day-average values for subsequent analysis. The 5-day averaged result was located on the last day of the 5-day period.

2.2 Observation data for model validation

In this study, the Bootstrap Sea Ice Concentrations (SIC) from Nimbus-7 SMMR and DMSP SSM/I-SSMIS (https://nsidc.org/data/nsidc-0079/versions/3) from the National Snow and Ice Data Center (NSIDC) (Comiso 2017; Markus and Cavalieri 2000) are used to validate the simulated sea ice concentration by FESOM. This dataset is available on a daily resolution with a horizontal resolution of 25 km by 25 km.

Sea ice production rate (SIP) estimated from the Advanced Microwave Scanning Radiometer-Earth Observing System (AMSR-E) product archived at the website (http://wwwod.lowtem.hokudai.ac.jp/polar-seaflux) is employed to evaluate the model simulated SIP. SIP is estimated from the AMSR-E data by the heat flux calculation using a thin-ice-thickness estimation algorithm and surface atmospheric data, with an assumption that the contribution of oceanic heat flux to sea-ice freezing/melting is negligible (Nihashi and Ohshima 2015; Nihashi et al. 2017; Ohshima et al. 2013; Tamura et al. 2016). Wind speed data at 10 m from the CORE-II forcing are compared with measured 10-m wind speed at Antarctic research stations near the coastal polynyas that this study is focused on, including the Zhongshan Station and the Mirny Station (Fig. 1). The wind speed measurements are available at the Reference Antarctic Data for Environmental Research (READER) project website (http://legacy.bas.ac.uk/met/READER). The measured winds are used along with the CORE-II forcing to select typical SOWEs.

2.3 Model validation

The performance of the FESOM model in capturing Antarctic coastal polynyas and simulating the ice production rates at these locations is evaluated by comparing the annual cumulative SIP from the model simulations with observations. Following Nihashi and Ohshima (2015), the calculation of annual cumulative SIP covers the period of March to October, i.e. the ice freezing seasons around Antarctica. A comparison of the annual cumulative SIP between the model simulation averaged over 2003–2008 and the
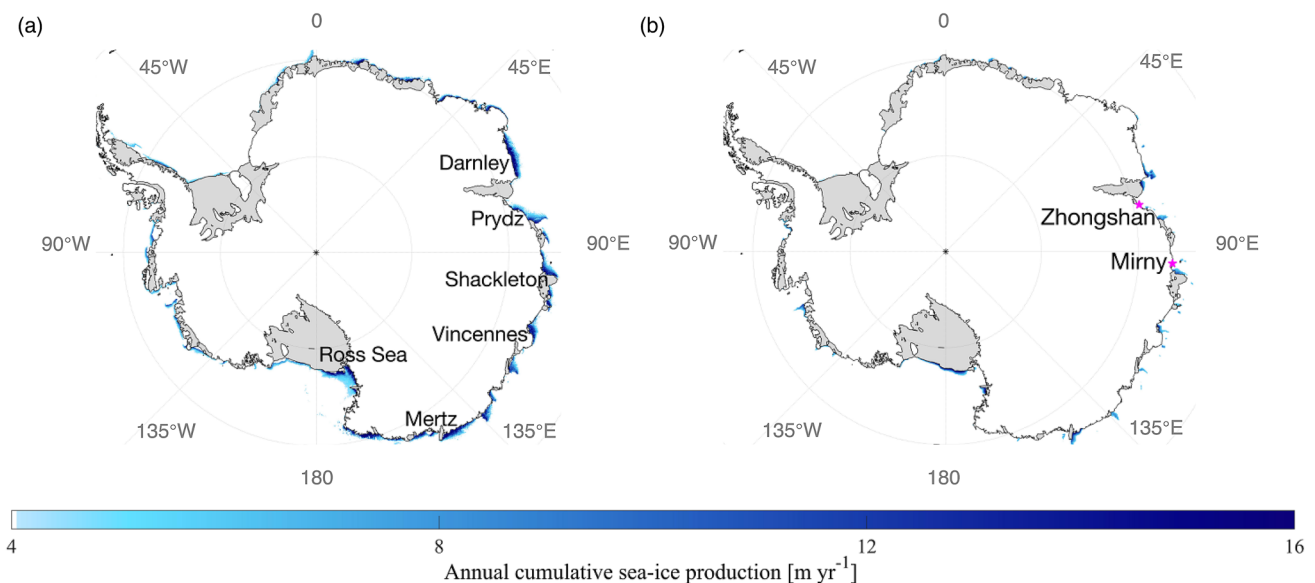

Fig. 1 Annual cumulative sea ice production rate over the continental shelf of Antarctica from **a** the FESOM simulation averaged over 2003–2008 and **b** the AMSR-E dataset averaged over 2003–2010

satellite-retrieved data averaged over 2003–2010 available at the website (http://wwwod.lowtem.hokudai.ac.jp/polar-seaflux) (Nihashi and Ohshima 2015) is presented in Fig. 1. It is first noted that the model well captures the locations of Antarctic coastal polynyas indicated by positive SIP values in the Ross Sea and along the East Antarctica coast. Compared to observations, the model overestimates SIP in the coastal polynyas. Overestimate of SIP compared to the estimate from satellite datasets is common to the Southern Ocean ocean-sea-ice models, possibly due to overestimate of sensible heat flux as a result of lack of coupling with atmosphere in the models and of the atmospheric forcing fields having low resolution. In addition, the overly smooth orography of the atmosphere model that has been used to produce the low-resolution winds (CORE-II) extends beyond the actual coastlines; this tends to overestimate the offshore winds, which in turn enhances SIP in coastal polynyas (Stössel et al. 2011). The simulated annual accumulative SIP from FESOM is consistent with results from other models used for studying Antarctic coastal polynyas (Kusahara et al. 2017; Zhang et al. 2015), ranging from 4 to 20 m year^{-1} depending on the location of the polynya and the distance from the coast within a specific polynya.

The statistical information of comparisons of 5-day-average SIC values in austral winter (June–September) averaged over Antarctic coastal polynyas from FESOM and from the SMMR-SSM/I microwave SIC product are provided in Table 1. Significant correlations ($P < 0.05$) between the modeled and observed SIC exist for all major coastal polynyas along East Antarctica and in the Ross Sea. The negative coefficient in Cape Darnley Polynya may result from the lack of data assimilated into the CORE-II product, as there is no surface research station near this polynya. In this study, we selected two polynyas characterized by the highest correlations (correlation coefficient $R > 0.5$ and $P < 0.0001$) to investigate the impacts of SOWEs on the sea ice and oceanic processes, that is, the Prydz Bay Polynya including the Davis and Barrier polynyas in the Prydz Bay ($R = 0.82$) and the Shackleton Polynya ($R = 0.64$), both of which are located

along the coast of East Antarctica (Fig. 1). The root mean square error (RMSE) of SIC for the Prydz Bay and Shackleton polynyas are 0.15 and 0.28, respectively, and the model tends to underestimate the SIC values. The underestimation for the Shackleton Polynya is relatively large, but as this study is focused on the variation of sea ice properties under changing winds, the significant and high correlation guarantees the ability of the model in capturing such temporal variability. Meanwhile, the correlation coefficients between the modeled and AMSR-E based monthly SIP for the Prydz Bay and Shackleton polynyas are 0.62 ($P < 0.001$) and 0.72 ($P < 0.0001$) respectively (Table 2), suggesting the temporal variability of SIP can be well simulated by the FESOM model. The Ross Sea Polynya is also noted by relatively good correlation between the modeled and observed SIC ($R = 0.46$), but there is a large positive bias of wind speed in the CORE-II product against measurements at the McMurdo Station for the Ross Sea Polynya (not shown), Therefore, this area is not included in the following analysis. The large positive wind bias is expected to induce larger underestimate of SIC relative to the satellite data, while in reality the RMSE of SIC is smaller than that of the other polynyas. This might result from an underestimate of the oceanic heat flux into the surface layer in the model, which causes less melting of sea ice (thus higher SIC) and compensates for the underestimate of SIC caused by unrealistically strong wind in the CORE-II forcing.

2.4 Methods

In this study, the coastal polynyas are defined as the areas where the multi-year average sea ice production rate from June to September is greater than zero based on the FESOM outputs. For each polynya, we selected 1 year during the FESOM simulation period that has high correlation between the wintertime CORE-II wind speed and observed wind speed and that is featured by a couple of typical SOWEs. The selected years for the Prydz Bay and Shackleton polynyas are 1998 and 2006, respectively. The threshold for

Table 1 The coefficient of correlation between the simulated and satellite passive-microwave SIC over June–September from 2005–2008, the p-value and the root mean square error (RMSE) of modeled SIC relative to observations

Polynya name	Correlation coefficient	P-value	RMSE
Prydz Bay	0.82	< 0.0001	0.15
Shackleton	0.64	< 0.0001	0.28
Ross Sea	0.46	< 0.0001	0.19
Vincennes Bay	0.29	< 0.005	0.27
Mertz Glacier	0.21	< 0.05	0.31
Cape Darnley	−0.25	< 0.05	0.35

Table 2 The coefficient of correlation between the simulated and AMSR-E based SIP over February–November from 2003 to 2006, the p-value and the root mean square error (RMSE) of modeled SIP relative to observations

Polynya name	Correlation coefficient	P-value	RMSE
Prydz Bay	0.62	< 0.001	1.07
Shackleton	0.72	< 0.0001	1.48
Ross Sea	0.82	< 0.0001	1.22
Vincennes Bay	0.69	< 0.0001	1.52
Mertz Glacier	0.57	< 0.001	1.29
Cape Darnley	0.83	< 0.0001	1.97

strong wind is the 80th percentile polynya-averaged wind speed, which are 10.8 m s^{-1} and 12.4 m s^{-1} respectively for the Prydz Bay and Shackleton polynyas. The influences of the SOWEs on sea ice and hydrographic properties are quantified by calculating the difference between polynya-area-averaged values under normal and strong wind conditions. The mixed layer depth (MLD) is defined as the depth where the potential density (σ_θ) anomaly differs by 0.03 kg m^{-3} from the surface potential density (Dong et al. 2008). HSSW is defined by the water mass with σ_θ above 28 kg m^{-3} (Yoon et al. 2020).

3 Results

3.1 The Prydz Bay Polynya

3.1.1 Sea ice response

Two representative SOWEs are selected for the Prydz Bay Polynya in the cold season of 1998: one from July 25 to August 9 (SOWE1) and one from August 9 to August 19 (SOWE2) (Fig. 2). The wind speed averaged over these two events were 13.6 m s^{-1} and 12.8 m s^{-1} at the Zhongshan Station respectively, both of them actually exceeded the 90th percentile wind speed. The temporal variation of the CORE-II wind speed was highly correlated with that of observation at the Zhongshan Station (R = 0.82, Fig. 2). Examination of the wind stress fields over the Prydz Bay Polynya and adjacent areas over 40 days covering the two SOWEs (Fig. 3)

shows that both of the two SOWEs were associated with the passage of synoptic- or meso-scale cyclones (Fig. 3d–g). At the peak of SOWE1 (July 30–August 4) and SOWE2 (August 14), the center of the corresponding cyclone sat just north of the Prydz Bay, and the southern branch of the cyclone dramatically enhanced the offshore wind component along the east coast of the polynya. After these two SOWEs, the center of the cyclone moved eastward out of the polynya region or was succeeded by a weaker cyclone (Fig. 3h–i). These wind patterns support the findings of Turner et al. (2009) and Weber et al. (2016) that extreme offshore wind speed over the coastal areas of East Antarctica is usually caused by the interaction of local topography and synoptic-scale cyclones. While these studies addressed the role of the western flank of cyclones in enhancing northward wind component that act as offshore wind for most of the East Antarctica coast, we found that the southern flank of cyclones are more important for increasing offshore (easterly) winds over polynyas that lie on the leeside of protruding topography.

Sea ice properties in the Prydz Bay Polynya showed notable sensitivity to the selected SOWEs (Figs. 4, 5). The mean offshore component of sea ice velocity (SIV) increased from 0.07 m s^{-1} prior to the SOWE1 (July 15–25, Fig. 4a–c in the polynya region) to 0.30 m s^{-1} at the onset of SOWE1 (July 30, Fig. 4d); the mean SIC decreased from 75 to 54% and SIP increased from 0.04 to 0.06 m day^{-1}. On August 4 when the center of the cyclone was located just offshore of the Prydz Bay, SIV along the east coast of the polynya remained high values of 0.22 m s^{-1}, and SIC in this area
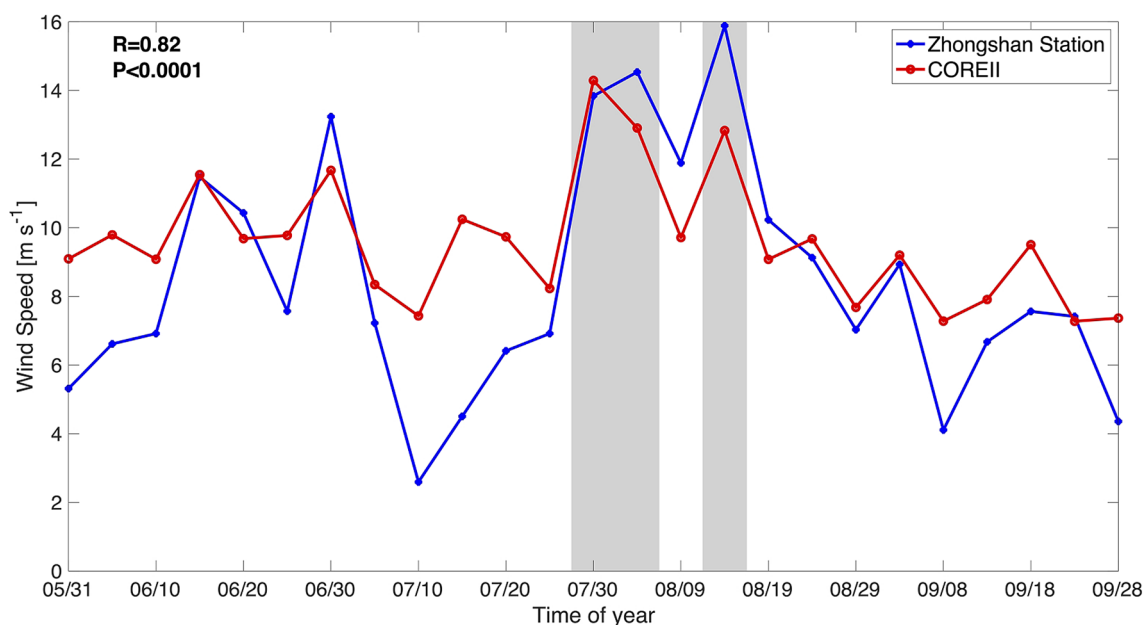

Fig. 2 Time series of 10-m wind speed at the Zhongshan Station from the CORE-II forcing and from observations during June to September of 1998. The gray shading represents the dates when SOWEs occurred in the Prydz Bay Polynya
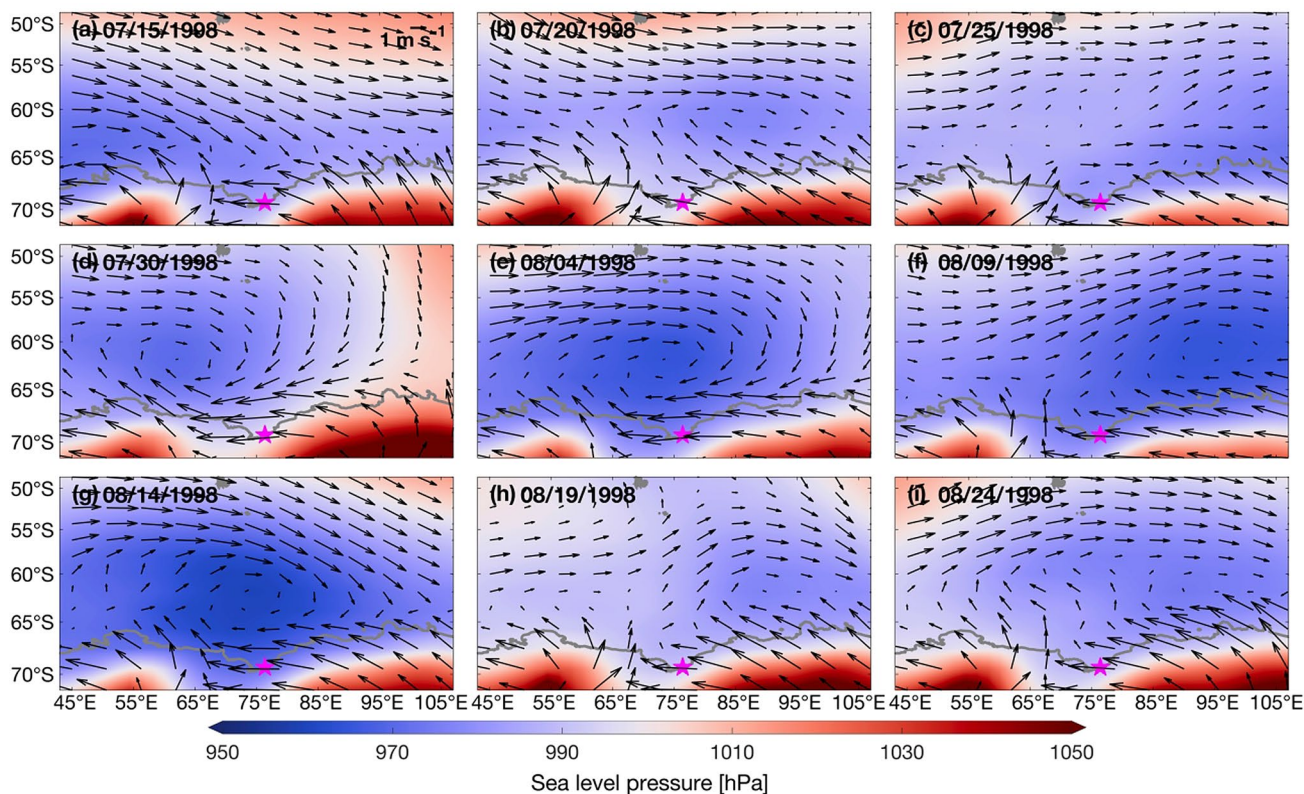
Fig. 3 a–i Spatial distributions of 5-day-average sea level pressure (color shading) and wind vectors (black arrow) near the Prydz Bay Polynya during July 15 to August 24 of 1998 that included two SOWEs. The magenta pentacle indicates the position of the Zhongshan Station

reached a minimum value of 44% (Fig. 4e). SIP increased up to twofold reaching about 0.09 m day^{-1} near the coastal region (Fig. 5e). On August 9, wind speed had dropped to a normal value of 9.7 m s^{-1} at the Zhongshan Station, but the coastal SIC remained low (Fig. 4f). The SIP field (Fig. 5f) responded timely to the wind speed reduction, and decreased to values only slightly higher than those prior to the onset of SOWE1.

On August 14, when SOWE2 developed associated with the passage of another cyclone, the area of low SIC expanded quickly (Fig. 4g), and a large portion of the polynya area was re-occupied by large SIP values above 0.08 m day^{-1} (Fig. 5g). Closely following the dramatic reduction of wind speed on August 19, SIP had basically recovered to the state before the two SOWEs, while the coastal polynya characterized by low SIC values is notably larger than that before the SOWEs. Therefore, for both of the two SOWEs, SIP demonstrated near-instantaneous response to the wind event. Also SIC responded fast, but the low values prevailed long, for about 5–10 days, which was also the case for sea ice thickness (SIT) during the two SOWEs (not shown).

The differences in wind speed and sea ice variables under normal and strong wind conditions are averaged over the Prydz Bay Polynya and summarized in Table 3. For SOWE1,

the wind speed was about two-fold larger than the normal values, i.e. from 7.0 to 14.0 m s^{-1}. SIV increased by 3.7 times reaching 0.26 m s^{-1}. SIC was reduced by about 26%, and SIP doubled to 0.08 m day^{-1}. For SOWE2, though the spatial-mean wind speed was only 12.1 m s^{-1} on August 14, the reduction of SIC and increase in SIP were still apparent in the polynya region, indicating that the SIC and SIP continued to be affected by the first event.

3.1.2 Oceanic response

An examination of surface salinity in the polynya region revealed that salinity kept increasing as a result of continuous sea ice formation following the SOWEs, and for such case the temporal variability of surface salinity is analyzed to study the impacts of SOWEs on the salinity field (Fig. 6). The surface salinity variability (SSV) for each date in Fig. 6 is obtained by subtracting the previous 5-day-averaged salinity from the average value on the current date. When SOWE1 was fully developed on July 30 (Fig. 6d), the most notable change in the SSV pattern occurred at the offshore edge of the polynya, where negative SSV values turned into positive values reaching 0.3 psu day^{-1} and above. On August 4 (Fig. 6e), the positive values spread to the coastal areas
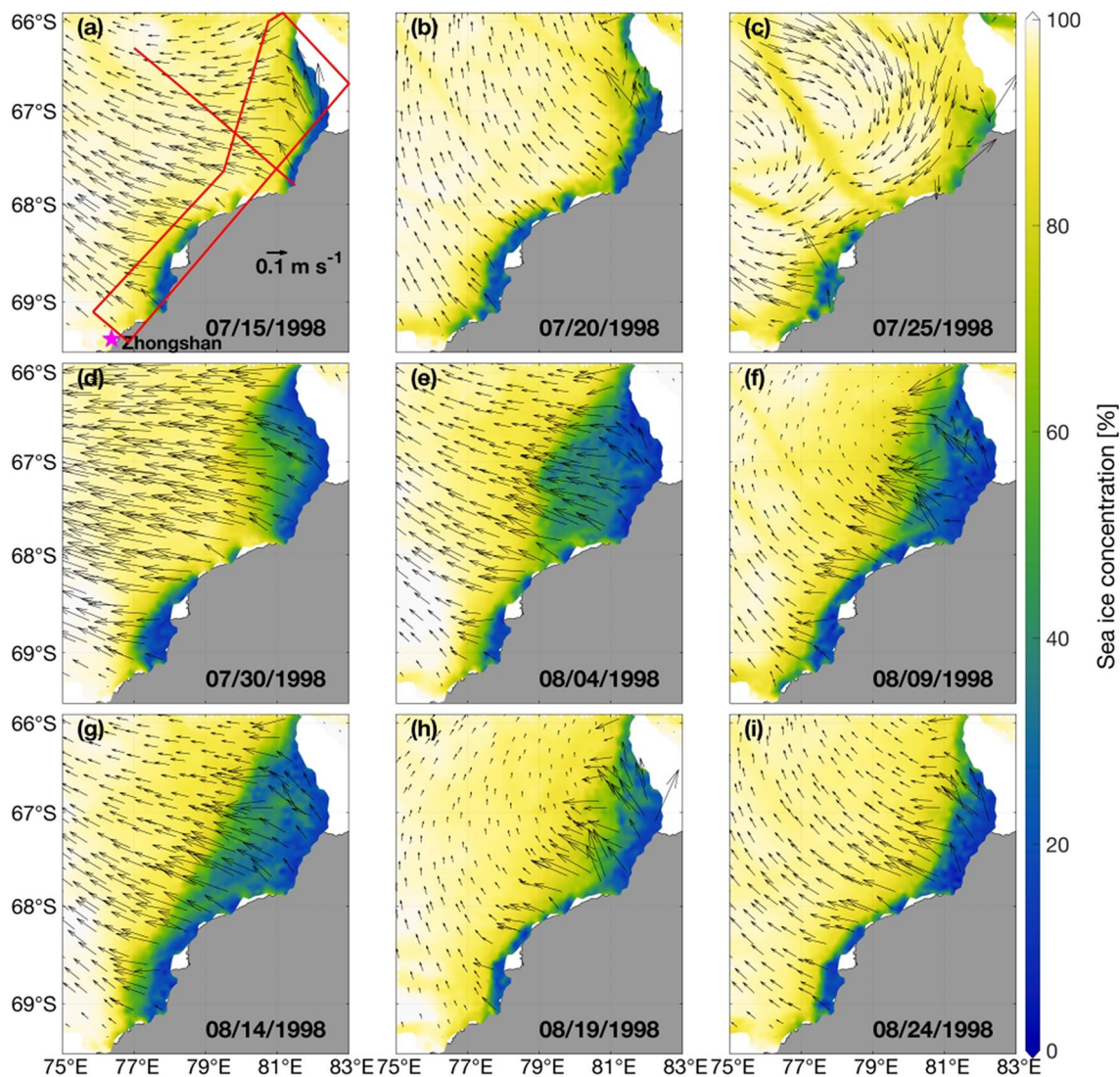
Fig. 4 a–i Spatial distributions of 5-day-average sea ice velocity (vector) and sea ice concentration (color shading) in the Prydz Bay Polynya and adjacent offshore areas during July 15 to August 24 of 1998 that included two SOWEs. In **a**, the magenta pentacle indicates the position of the Zhongshan Station, the red line indicates the location of the selected cross-shelf transect, and the polygon indicates the defined polynya region

in the northeastern section of the polynya. As wind speed dropped to normal values on August 9, SSV turned nearly to zero at the edge of the polynya, while along the east coast positive SSV values dominated a larger area. For SOWE2 on August 14 (Fig. 6g), there was a slight increase in SSV values, which were about 0.01 psu day^{-1} larger than those on August 9. Positive SSV was still detected along the coast on August 19 (Fig. 6h), and on August 24 (Fig. 6i) SSV had gradually recovered to the state prior to the two SOWEs (as on July 25).

Responding to the onset of SOWE1, within the polynya MLD increased from 10–50 m on July 25 to 50–150 m on August 4 (Fig. 7e). The most notable change occurred near the edge of the polynya, i.e. the area of largest change

in SSV, where MLD increased by approximately 200 m. MLD in the polynya was slightly reduced on August 9, and then quickly increased to 100–150 m under SOWE2 on August 14, and further increased on August 19. The quick increase in MLD responding to the development of a SOWE possibly resulted from the enhanced wind-induced mixing, and the phenomenon that the impact of a SOWE on MLD persisted for a few days seemed associated with the lag response of convection to the SOWE, which will be discussed later in this section. More details about the distinction of spatial-mean hydrographic variables in the Prydz Bay Polynya between the normal and extreme atmospheric conditions are given in Table 3. For these two SOWEs, SSV increased by 75% and 50% reaching
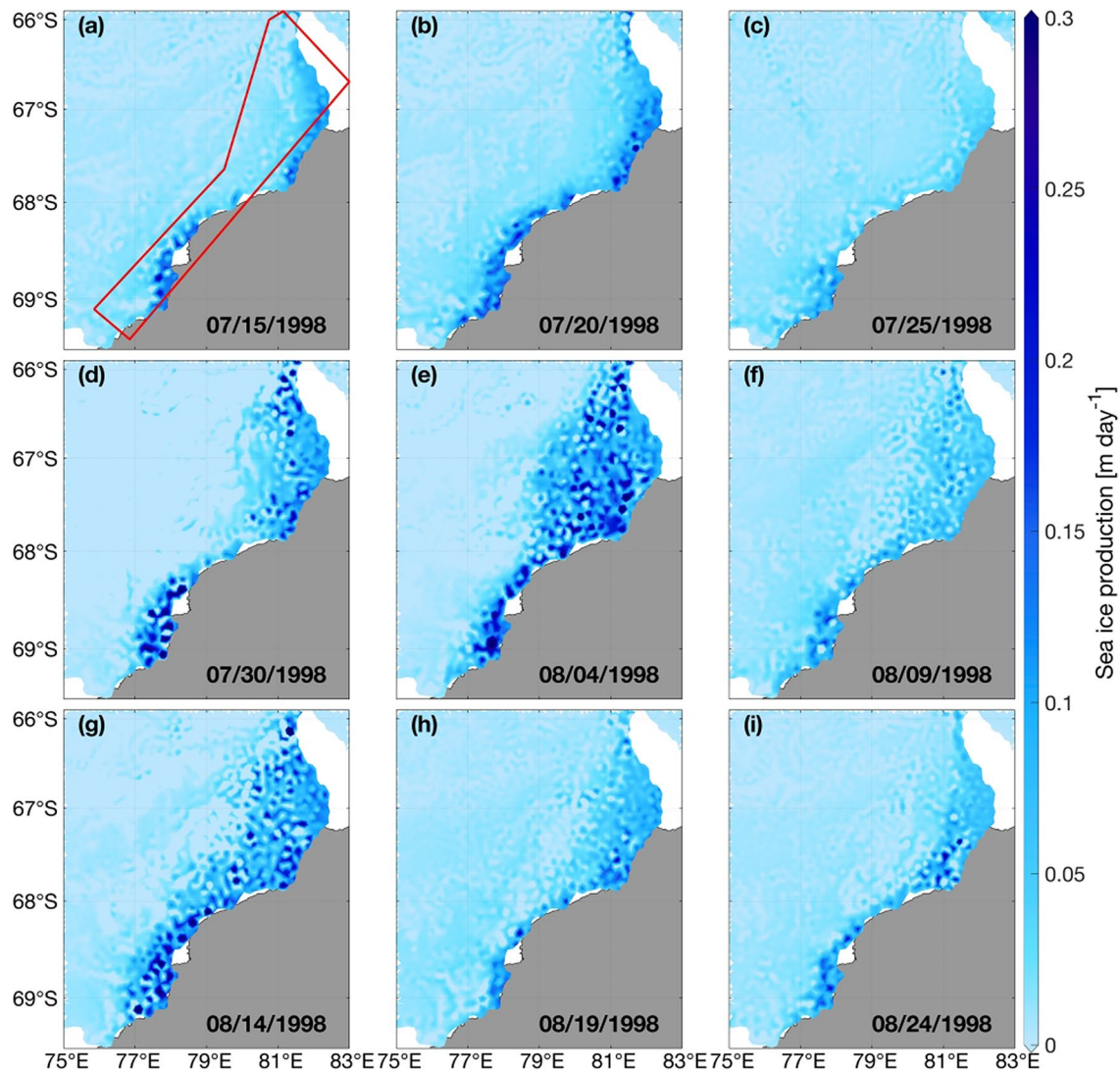
Fig. 5 Same as Fig. 4 but for sea ice production

Table 3 Comparisons of polynya-averaged sea ice and oceanic properties under normal wind forcing and SOWEs for the Prydz Bay Polynya. The normal values are calculated as the polynya-averaged, time-mean values over July 15–July 25 in 1998 prior to the SOWEs

Properties	Normal	SOWE1	SOWE2
Wind speed (m s^{-1})	7.0	14.0	12.1
Sea ice velocity (m s^{-1})	0.07	0.26	0.21
Sea ice concentration	0.75	0.49	0.38
Sea ice production (m day^{-1})	0.04	0.08	0.08
Surface salinity variability (psu day^{-1})	0.04	0.07	0.06
Mixed layer depth (m)[a]	80	87	103

[a]The calculation was performed over the period of SOWEs with a 5-day lag because there was a lag response of MLD to SOWEs

0.07 and 0.06 psu day^{-1} respectively. MLD also increased noticeably with an area-average value of 87 m and 103 m respectively during these two SOWEs.

The vertical profile of σ_θ along the cross-shelf section noted in Fig. 4a shows the presence of HSSW ($\sigma_\theta >$ 28.0 kg m^{-3}) on the continental shelf deeper than 800 m (Fig. 8h–i). The circulation patterns are superimposed in Fig. 8. After the onset of SOWE1 on July 30, vertical motions near the coast were downslope, compared to the alternative upslope and downslope motions prior to the SOWE. The downward motions reached the greatest strength on August 9 when wind had reduced, and there was a slight increase in σ_θ of the coastal water at 100–500 m compared to July 30, suggesting that coastal convection and the formation of HSSW lagged the SOWE by 5 days or more. The lag response of convection could
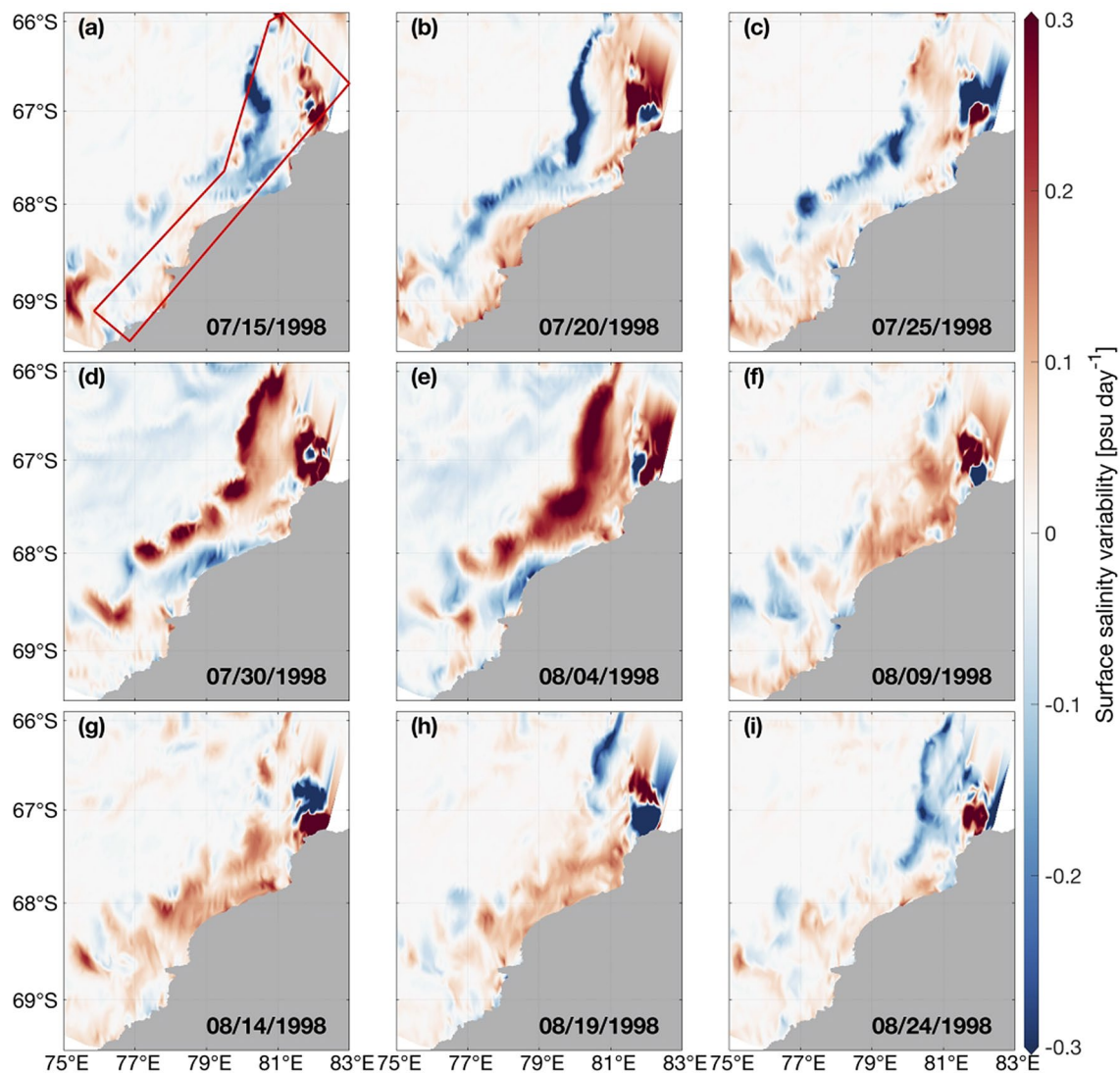
Fig. 6 Same as Fig. 4, but for the surface salinity variability which is calculated by subtracting the previous 5-day-average salinity from the value on the current date

also explain why MLD was still large on August 9 when winds were weak. At SOWE2 (August 14), the weak coastal convection and HSSW characteristics still exhibited the footprints of weak wind on August 9, and the impact of SOWE2 was reflected in the strengthening of coastal convection on August 19 which was consistent with the MLD increase along the coastline. It is noted that on August 19–24 HSSW was formed near the coast at the depth of 300–800 m, accompanied by an anti-clockwise circulation that was developed near the front created by the HSSW and offshore water. There was no significant

change in the HSSW characteristics in the deep layers below 800 m.

3.2 The Shackleton Polynya

3.2.1 Sea ice response

The SOWE chosen in the Shackleton Polynya was from July 30 to August 9 of 2006, when the wind speed reached 12.6 m s^{-1} at the Mirny Station and was above the 80th percentile (Fig. 9). The wind speed from the CORE-II forcing had a low bias compared to the observed values,
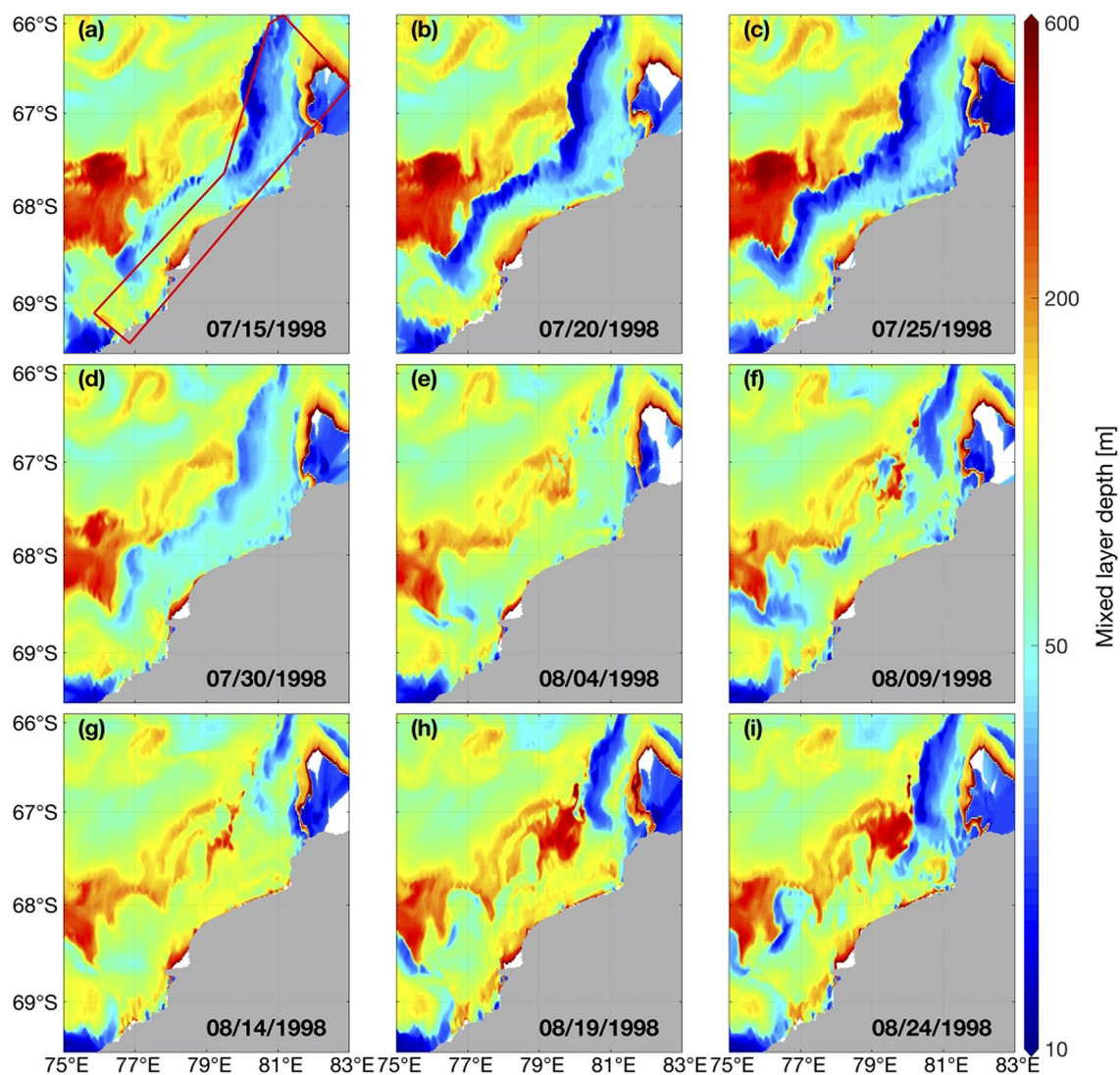
Fig. 7 Same as Fig. 4 but for the mixed layer depth

which possibly results from inadequate representation of small-scale wind due to the coarse resolution of this product. The wind stress and sea level pressure fields (Fig. 10) show that the SOWE was also associated with the passage of a synoptic-scale cyclone, which moved eastward and sat offshore of the Shackleton Polynya on August 4 (Fig. 10c).

As shown in Fig. 11, before the SOWE, the offshore component of SIV was only large in the coastal regions possibly influenced by local katabatic winds (Fig. 11a, b). On August 4, high SIV greater than 0.18 m s^{-1} prevailed over the entire polynya and regions nearby (Fig. 11c), and low SIC values initially present along the east coast spread to offshore areas and along the south coast. Positive SIP values emerged over nearly the entire polynya with a mean value of 0.11 m day^{-1} (Fig. 12c). Following the reduction of wind speed during

August 9–19, SIV decreased quickly in the offshore areas (Fig. 11d–f). Large SIV still existed in the coastal regions on August 9 when the Shackleton Polynya was located on the western side of the cyclone and the offshore wind remained a moderate magnitude, and the coastal SIC values exhibited further decrease. SIP followed the SIV change closely and showed a noticeable decrease relative to the values on August 4. On August 14–19, the strong offshore motion of sea ice was confined at a few locations near the coast, while low SIC values persisted all along the coast. SIP was still positive along the coast on August 14, but by August 19 SIP had reduced to the level prior to the SOWE (as on July 30). The facts that both SIV and SIC responded fast to the SOWE but low SIC values prevailed long after the SOWE are similar to the situation in the Prydz Bay Polynya. In the
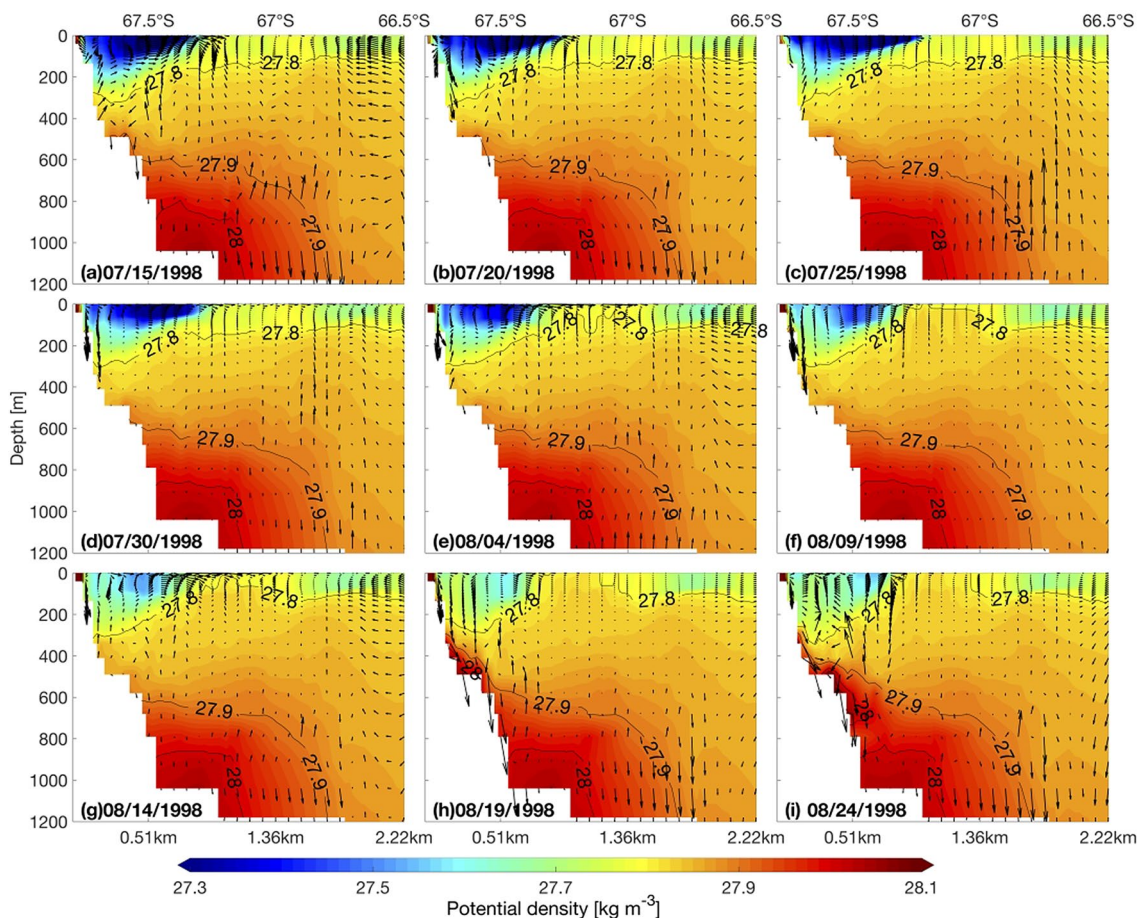
Fig. 8 **a–i** Vertical transects of potential density (color shading) and circulation (vector) for the cross-shelf transect indicated by the red line in Fig. 4a during July 15 to August 24 of 1998. The black contour lines indicate isopycnals at an interval of 0.1 kg m^{-3}
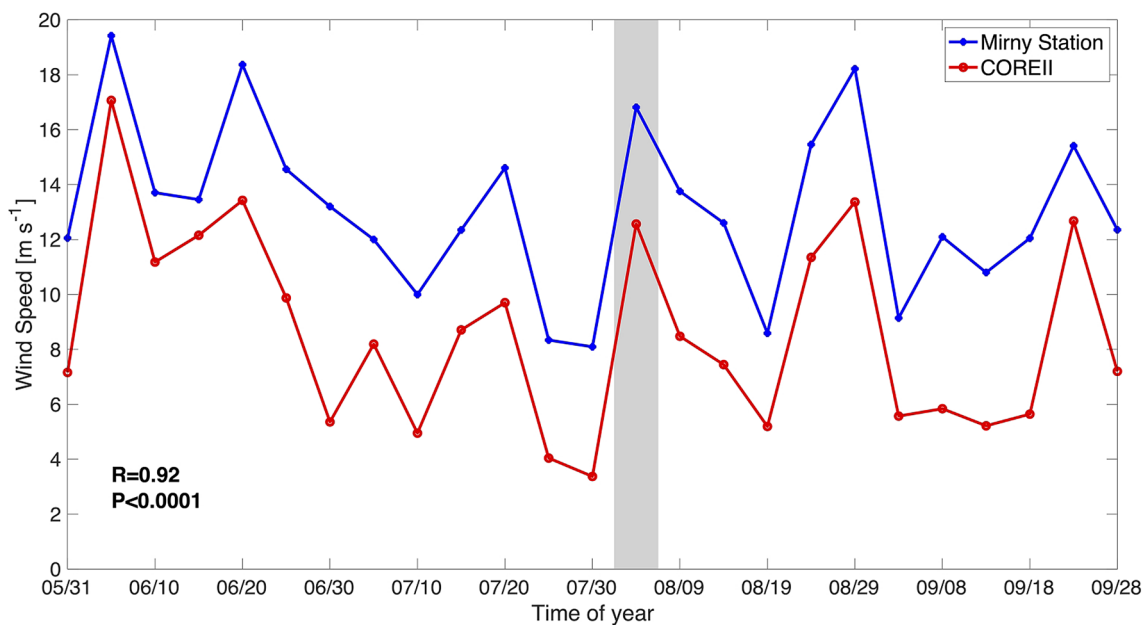
Fig. 9 Time series of 10-m wind speed at the Mirny Station from the CORE-II forcing and from observations during June to September of 2006. The gray shading represents the date when SOWE occurs in the Shackleton Polynya
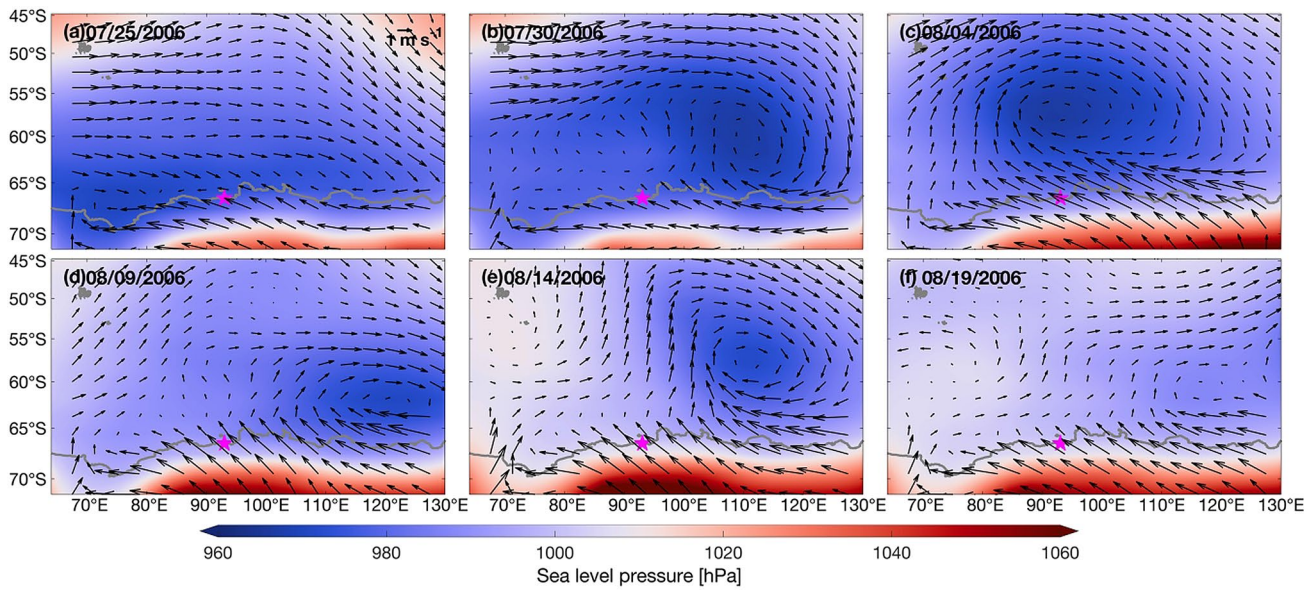
Fig. 10 a–f Spatial distributions of 5-day-average sea level pressure (color shading) and wind vector (black arrow) near the Shackleton Polynya during July 25 to August 19 of 2006 that included one SOWE. The magenta pentacle indicates the position of the Mirny Station
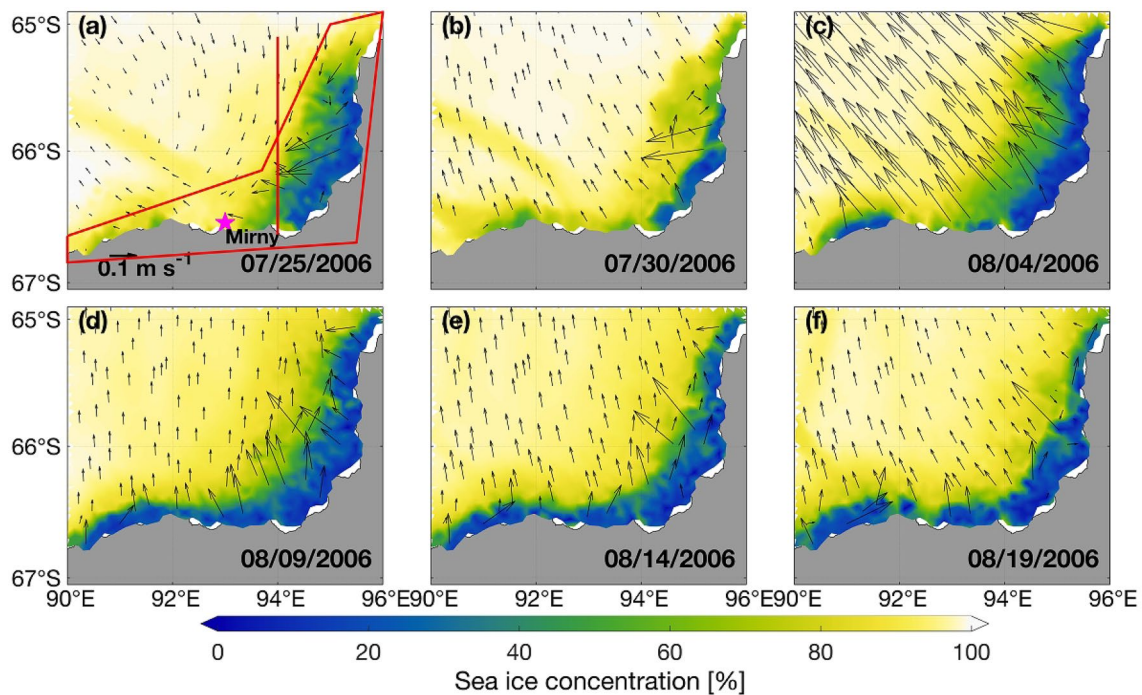
Fig. 11 a–f Spatial distributions of 5-day-average sea ice velocity (vector) and sea ice concentration (color shading) in the Shackleton Polynya and adjacent offshore areas during July 25 to August 19 of 2006 that included one SOWE. In **a**, the magenta pentacle in indi- cates the position of Mirny Station, the red line indicates the loca- tion of the selected cross-shelf transect, and the polygon indicates the defined polynya region

Shackleton Polynya, low SIC persisted for 10–15 days or even longer, and high SIP persisted for 5–10 days.

The differences in wind speed and sea ice variables under normal conditions and the selected SOWE, aver- aged over the Shackleton Polynya, are given in Table 4. The
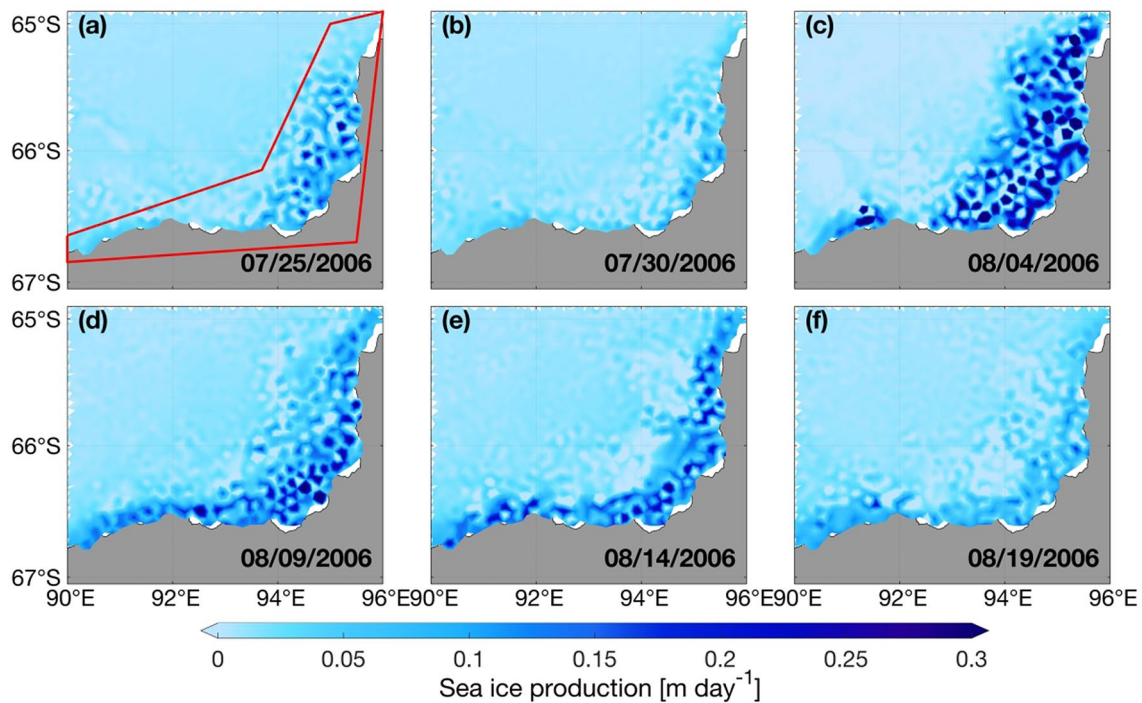
Fig. 12 Same as Fig. 11 but for sea ice production

Table 4 Comparisons of polynya-averaged sea ice and oceanic properties under normal wind forcing and the SOWE for the Shackleton Polynya. The normal values are calculated as the polynya-averaged, time-mean values over July 25–July 30 in 2006 prior to the SOWE

Properties	Normal	SOWE
Wind speed (m s^{-1})	4.2	12.8
Sea ice velocity (m s^{-1})	0.04	0.18
Sea ice concentration	0.69	0.48
Sea ice production (m day^{-1})	0.03	0.11
Surface salinity variability (psu day^{-1})[b]	− 0.03	0.05
Mixed layer depth (m)[a]	151	206

[a]The calculation was performed over the period of SOWE with a 10-day lag because there was a lag response of SSV and MLD to SOWEs

area-averaged wind speed increased by almost 3 times during this SOWE. The area-averaged SIV showed more than a four-fold increase, reaching 0.18 m s^{-1}, and SIP showed an almost four-fold increase, but SIC reduced only slightly. The relative increases in the wind speed, SIV and SIP were larger than those found in the Prydz Bay Polynya (Table 3), but the relative decrease in SIC was smaller, suggesting that SIC was affected by other processes in addition to the wind-driven ice drift, such as the feedback from the SIP change and change in ocean currents.

3.2.2 Oceanic response

The spatial patterns of SSV and MLD are displayed in Figs. 13 and 14, respectively. At the peak of the SOWE on August 4 (Fig. 13c), there was a slight increase in the coastal SSV values compared to those on July 30. SSV increased significantly and virtually occupied the entire polynya region on August 9 (Fig. 13d), with the area-averaged value reaching 0.08 psu day^{-1}. Consistent with the SSV change, MLD also showed a noticeable increase on August 9 (Fig. 14d), larger than that on August 4 and before (Fig. 14a–c). SSV remained high on August 14 (Fig. 13e) and then recovered to the state at the onset of SOWE (Fig. 13f). MLD also remained high (Fig. 14e), with the area-averaged mean of 227 m, and then reduced to 190 m on August 19 (Fig. 14f). Compared to the Prydz Bay Polynya, SSV and MLD in the Shackleton Polynya have a longer lag in response to the SOWEs.

The potential density and circulation distributions on the cross-shelf transect along 94° E (Fig. 11a) in the Shackleton Polynya are shown in Fig. 15. Two circulations cells seemed to persist above 500 m: one counterclockwise circulation near the coast and one clockwise circulation in the area of 66.3° S–66.1° S. Similar to the situation in the Prydz Bay Polynya, after a few days of the SOWE on August 4, enhanced downward motions were observed in the coastal area (August 9), which was followed by a noticeable increase in the σ_θ of the HSSW from surface to 400 m along the coast.
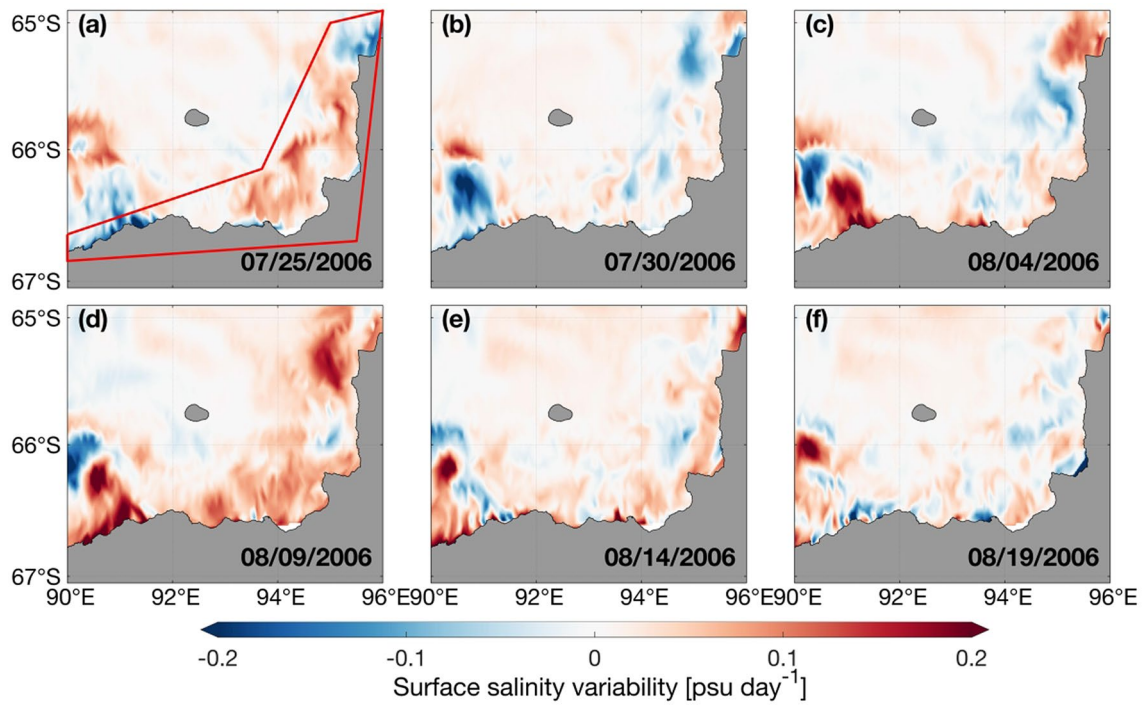
Fig. 13 Same as Fig. 11, but for the surface salinity variability
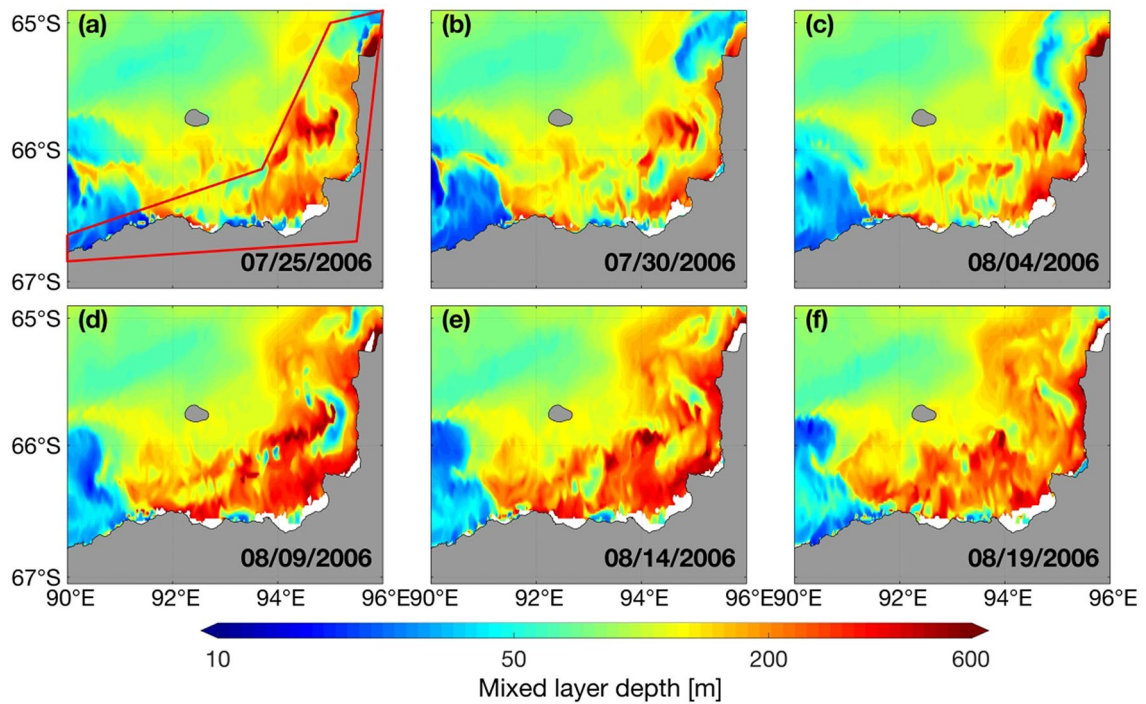

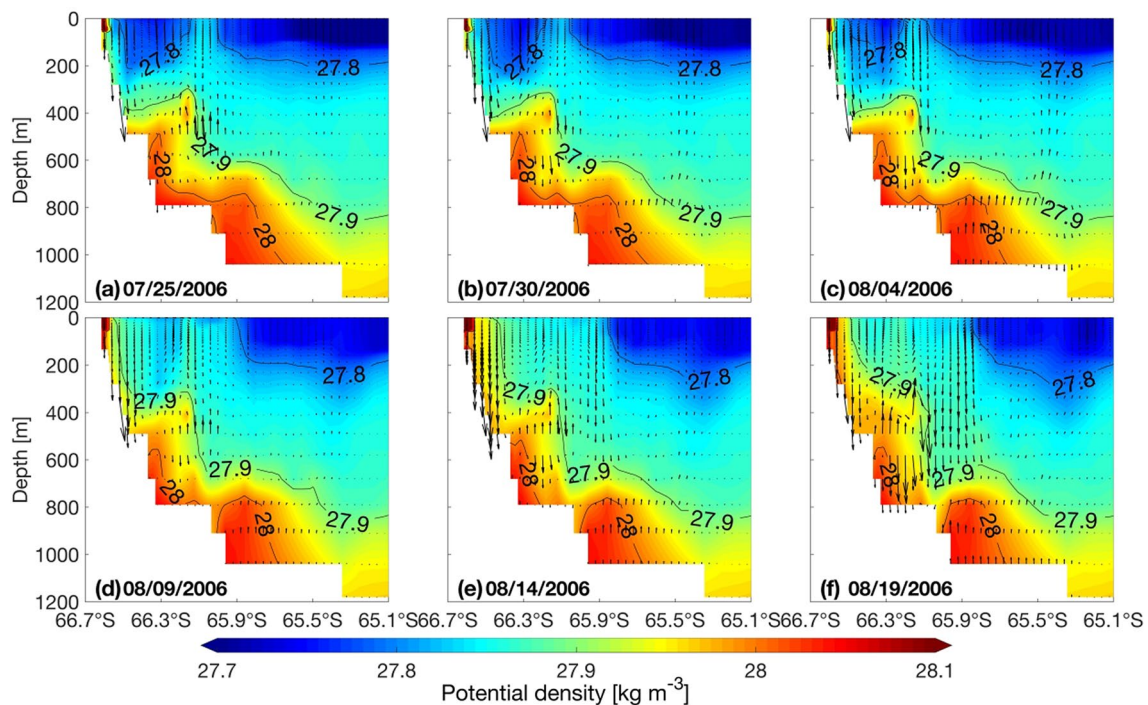**Fig. 14** Same as Fig. 11, but for the mixed layer depth

Fig. 15 **a–f** Vertical transects of potential density (color shading) and circulation patterns (vector) at 94°E during July 25 to August 19 of 2006. The black contour lines indicate isopycnals at an interval of 0.1 kg m^{-3}

Convection reached the maximum strength on August 14 and weakened on August 19 when the wind was reduced, while σ_θ kept increasing during August 14–19 and HSSW characterized by high potential density at 0–400 m expanded offshore. Same as the case in the Prydz Bay Polynya, the HSSW characteristics during the SOWE and a few days after were not remarkably affected by the wind event in the deep layers below 600 m.

3.3 The relative significance of wind speed and air temperature during SOWEs in sea-ice variations

During SOWEs, sea ice formation in Antarctic coastal polynyas is due to the combined effects of strong winds and cold, dry air, which contribute to larger heat loss from the sea surface via turbulent fluxes of sensible and latent heat and negative net longwave radiation. If this heat loss is not balanced by the oceanic heat flux, the sea surface cools and finally freezes. In Antarctic coastal polynyas, the latent heat flux is much smaller than the sensible heat flux (Launiainen and Vihma 1994), and therefore we do not address the effects of air moisture. To elucidate the relative role of wind speed and air temperature on sea ice formation in the polynya regions, linear regression of sea ice variables onto the two atmospheric quantities over the two polynyas is implemented over the period

of June–September during 1988–2008, and the results are presented in Fig. 16. For the Prydz Bay Polynya, SIC is both significantly and negatively correlated with the wind speed and air temperature, with the correlation to wind (R = − 0.61, P < 0.0001) higher than that to air temperature (R = − 0.53, P < 0.0001). The relationship of SIT with wind and air temperature shows a resemblance to those for SIC. SIP is highly, positively correlated with wind speed (R = 0.78), while the correlation with air temperature is quite weak (R = 0.24). Results for the Shackleton Polynya are similar to those for the Prydz Bay Polynya, with SIC being significantly correlated with both wind speed (R = − 0.52, P < 0.0001) and air temperature (R = − 0.35, P < 0.0001) while SIP only well correlated with wind speed (R = 0.67, P < 0.0001). Variations in air temperature associated with atmospheric processes other than the wind events could also play a role in the SIC change, and this may explain why both SIP and SIC exhibited almost instantaneous responses to the SOWEs but low SIC values prevailed long after the events (see Sect. 4.2). The results that sea ice properties in the polynyas are more correlated with wind than with air temperature are consistent with the conclusions from Ding et al. (2020), which is focused on the Terra Nova Bay Polynya in the Ross Sea using satellite observations and atmospheric reanalysis. This study showed that in low air-temperature intervals (below ~ − 25 °C), the area of the polynya is more closely correlated with the air temperature change than wind speed, while in moderate-to-high air

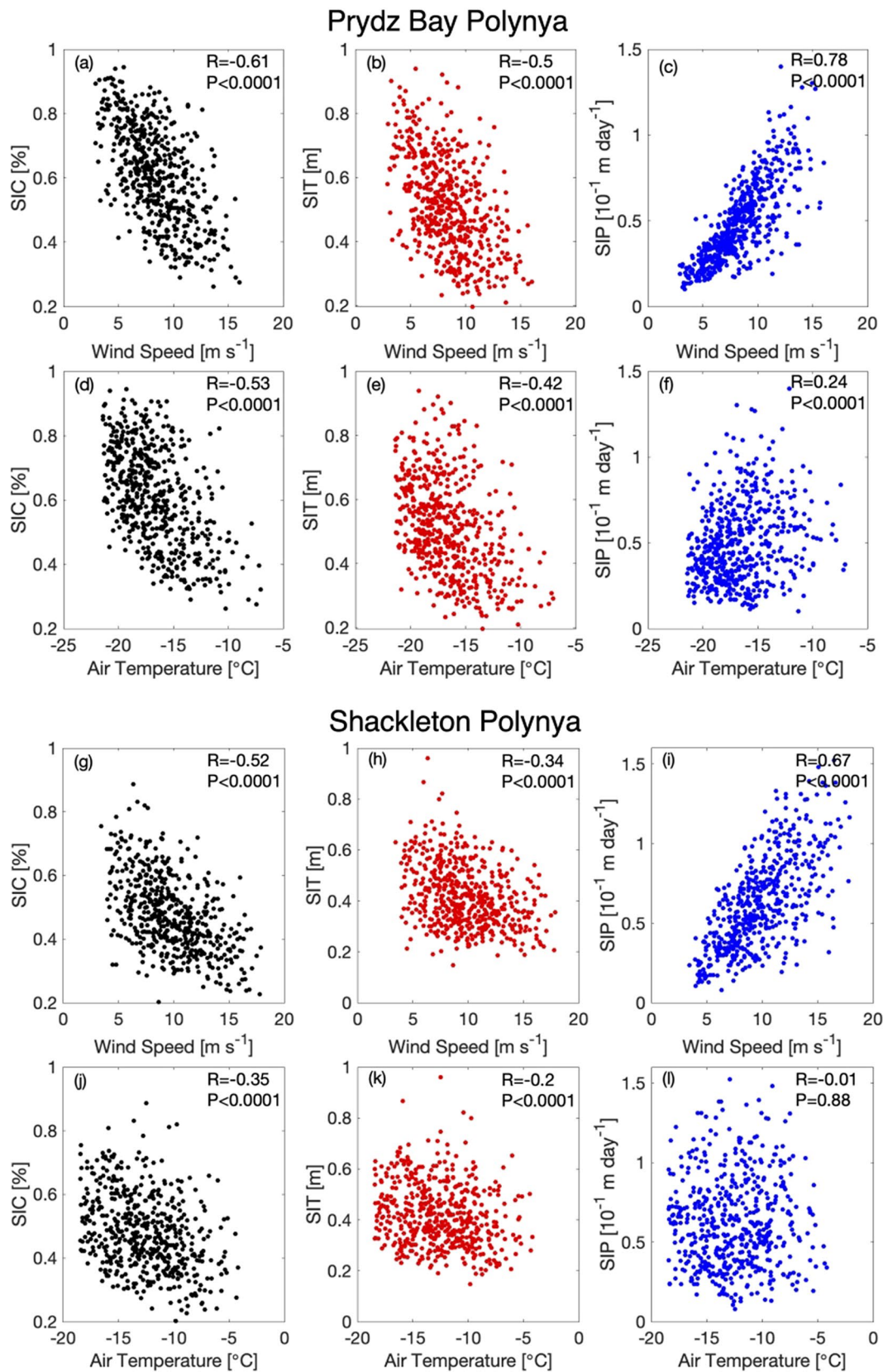**Fig. 16** Linear relationship of **a**, **d** SIC, **b**, **e** SIT and **c**, **f** SIP with **a–c** 10-m wind speed and with **d–f** 10-m air temperature from June to September during 1988–2008 in the Prydz Bay Polynya. **g–l** Same as **a–f** but for the Shackleton Polynya

temperature intervals (above $-25\,°C$), the range where air temperature near the Prydz Bay and Shackleton polynyas fall in, the change in polynya area is more related to wind.

4 Discussion

4.1 The relative role of variations in local katabatic wind and cyclones in change of offshore wind speed

It is generally considered that the coastal katabatic wind plays a major role in driving the formation of Antarctic coastal polynyas and sea ice formation. Katabatic wind is traditionally defined as a downslope cold flow driven by gravity and pressure gradient force on a sloping surface near the Antarctica coast, and its direction is controlled largely by topography (Lutgens and Tarbuck 2001). The katabatic wind occurs in the lowermost tens or a few hundreds of meters of the atmosphere (Vihma et al. 2011). Theoretically, the nominal 1° resolution of the CORE-II product is not adequate to resolve the local katabatic winds in regions of a complex orography, and this could be the reason for the low bias of CORE-II wind speed compared to the observed wind speed near the Shackleton Polynya (Fig. 9), though the assimilation of Antarctic weather station data into CORE-II should have reduced such bias. In this study, we have also tried to select the polynyas characterized by the highest correlations between the CORE-II wind and observed wind as well as between the modeled and observed sea ice properties, in order to minimize errors from the model. On the other hand, a wider definition for katabatic wind is any downslope wind off the Antarctic continent (Ahrens 2000), in which the component contributed by synoptic wind is included. In this context, our study actually focused on the variation of the katabatic wind component associated with the synoptic wind. An exploration of the role of a wind event purely related to local (narrow-definition) katabatic wind on Antarctic coastal polynyas needs employing high-resolution atmospheric forcing products, such as the ECMWF global operational forecasting system, presently available with 9 km horizontal resolution, or the regional Antarctic Mesoscale Prediction System (AMPS) that has a spatial resolution of 10 km or even higher to force the ocean-sea-ice model. But on the other hand, we actually compared the CORE-II forcing with the ERA5 reanalysis product, which has a higher horizontal resolution of 0.25° by 0.25°, and found that the spatial distributions of sea level pressure and wind vectors from the two products exhibited very similar patterns near the Prydz Bay and Shackleton polynyas (Figs. 17a–i, 18a–f). It is noted that near the Prydz Bay Polynya, wind along the coastline is

larger in the lower-resolution CORE-II product compared to ERA5 (Fig. 17j), which is consistent with the findings revealed of Stössel et al. (2011). For the Shackleton Polynya, such feature was not found (Fig. 18g). The correlations of the polynya-averaged wind speed from CORE-II and ERA5 over the Prydz Bay and Shackleton polynyas are in excess of 0.9 (P < 0.0001), respectively. For this study, the temporal change of the coastal wind is more important information than the absolute value of wind. For both polynyas, time series of the temporal change of wind (difference in wind values from two consecutive time steps) from CORE-II and ERA5 largely overlap each other (Figs. 17k, 18h), suggesting that the resulting temporal change in sea ice and oceanic properties should also be similar when using ERA5 winds instead of CORE-II winds as wind forcing.

It is also noted that this study employs the 5-day-average CORE-II forcing data. By examining the daily CORE-II atmospheric fields, we found that the time span of synoptic-scale events over the study areas over the 5-day period varied from 2 days up to 7 days. For events lasting for 2–3 days (which occur less frequently compared to those lasting longer), there are two cyclones passing by the study areas, and the averaged field is either a reflection of the stronger event or the interactive result of the two cyclones. If the latter case happens, we would expect more details in the sea ice response in the 5-day period, which cannot be resolved from the 5-day-average sea ice fields. But as revealed from Fig. 16, there exists an almost linear relationship between sea ice properties (SIC and SIP) and wind speed, indicating that the 5-day averaged SIC field reflects the response to the 5-day averaged wind field that spans over two cyclone events. As discussed above, the oceanic response reflects cumulative effects of wind events, and therefore we would not expect significant differences in the change of oceanic quantities from using 5-day-average forcing and daily forcing.

4.2 The response time of sea ice variables to SOWEs

It is noted that different sea ice variables have different response time to the SOWEs. SIV showed instantaneous response to the wind change, which is consistent with earlier studies. For example, in free-drift conditions the typical response time of ice velocity to wind forcing is a few hours (Zubov 1945). The response of SIP is also fast. SIP is affected by the wind, air temperature, and air specific humidity. The opening of coastal polynyas is controlled by the wind, and the magnitude of the turbulent heat loss from the polynyas is mostly controlled by the wind speed and air temperature (assuming that the sea surface temperature remains close to the freezing point). Results in Sect. 3.3 show that for SIP, it is only significantly correlated with wind speed,
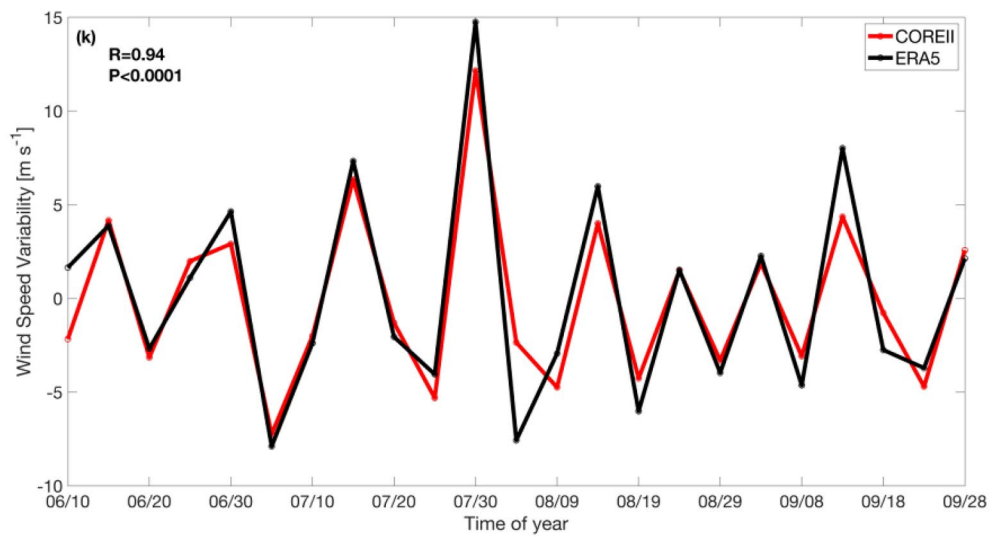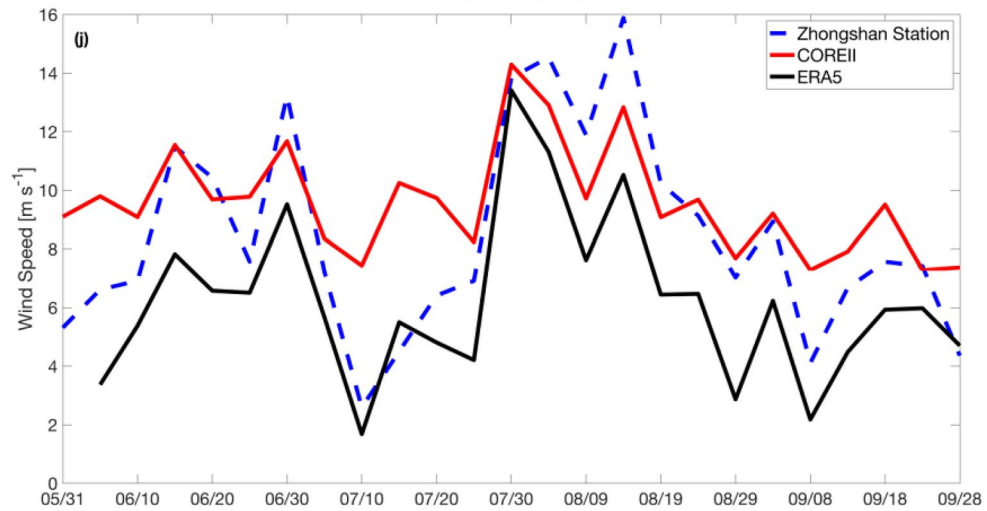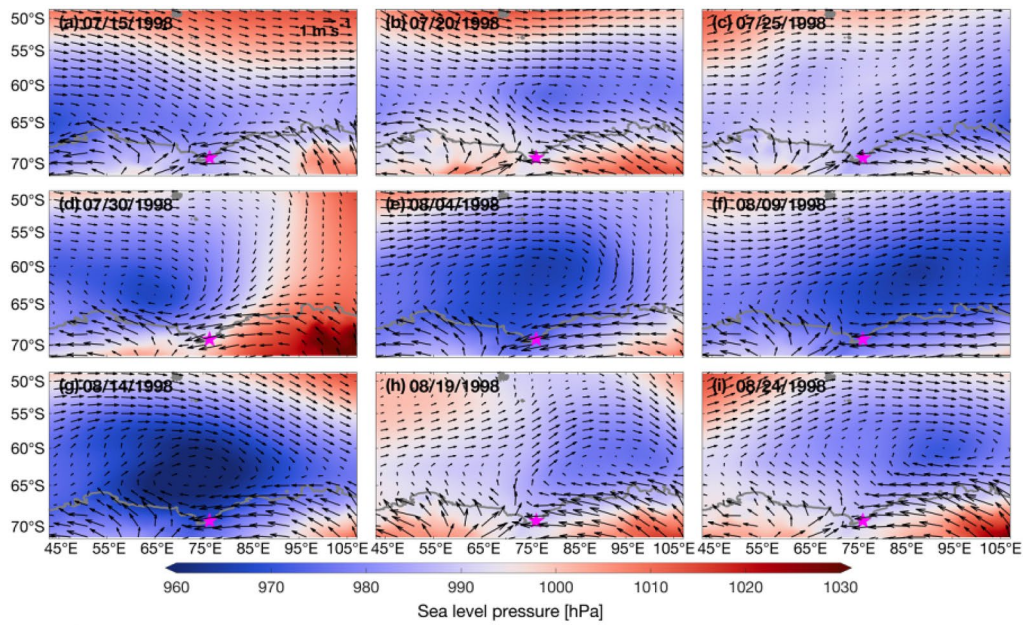
and not with air temperature. This is natural, as strong winds favor both opening of polynyas (Fig. 16a, g) and a large heat loss from them, driving SIP. The lack of correlation between SIP and air temperature could result from compensating effects: cold air is needed for a large heat flux from a polynya, resulting in a large SIP, but this upward flux heats the air and, accordingly, air temperatures are higher under the occurrence of a coastal polynya than in cases of high ice concentration (Fig. 16d, j).

For both polynyas, the results indicate that the low SIC prevailed some 5–15 days after the SOWEs. After the SOWEs, the thermodynamic growth of new ice in the polynya is expected to increase the ice concentration. This is because sea ice growth is a slow process; the typical growth rates observed by Smith et al. (2012) near Antarctic ice shelves were less than 0.01 m day^{-1}. Therefore, the SIC increase from thermodynamic ice growth cannot immediately compensate for the SOWE-induced SIC reduction, resulting in the persistence of low SIC values. Additionally, although SOWEs favor the opening of coastal polynyas, the wind following SOWEs, though weaker, was still offshore and drove offshore ice transport (Figs. 4, 11), and as such SIC in the polynyas cannot immediately recover to the level of the smaller-polynya state prior to the SOWEs. Moreover, we found that air temperature rose quickly after some SOWEs (not shown), which can also contribute to the persistence of low SIC in the relatively calm wind condition.

4.3 Seasonal-scale effects of the SOWEs on HSSW formation

Our analysis shows that for both the Prydz Bay and Shackleton polynyas, SOWEs have eminent influences on the HSSW formation in the layers above 800 m, while in the deeper layers the HSSW features do not change. This is possibly due to the fact that it takes a longer time for the deep HSSW to adjust to the SOWEs, and the high-frequency SOWEs obscure the response of HSSW to any single wind event. As such, HSSW in the deep layers would reflect the cumulative effects of SOWEs in the winter season. For each of the two polynyas, winter seasons from 2 years with contrasting SOWE duration are selected, and HSSW accumulation in the deep layers is compared. For the Prydz Bay Polynya,

1998 and 2005 are chosen as the years with long- and short-duration of SOWE, which respectively have a cumulative duration of SOWE in winter of 27 and 19 days and an average wind speed of 13.62 m s^{-1} and 13.52 m s^{-1}. Vertical transects of the average potential density over winter on the cross-shelf section and a section along 80°E are displayed in Fig. 19. Both of the two sections show that there was an apparent occupation of HSSW ($\sigma_\theta > 28.0$ kg m^{-3}) at the depth of 800–1200 m in 1998 (Fig. 19a, c), while in 2005 HSSW was barely observed in the deep layers (Fig. 19b, d). The fact that the average wind speed over winter is similar in these 2 years demonstrated the role of SOWE duration in HSSW formation in the deep ocean near the polynya regions. For the Shackleton Polynya, 2006 and 2004 are chosen as the years long- and short-duration of SOWE respectively, which respectively have a wintertime duration of SOWE of 29 and 19 days and an average wind speed of 15.95 m s^{-1} and 15.33 m s^{-1}. Vertical transects of the average potential density over winter on the cross-shelf sections along 94°E and 95°E are shown in Fig. 20. For both of the two sections, HSSW occupied the coastal region at a depth of 300–1000 m in 2006 (Fig. 20a, c), and in 2004 there was virtually no presence of HSSW (Fig. 20b, d). This again suggests the importance of SOWE occurrence in the HSSW formation and accumulation in the deep ocean in Antarctic coastal polynyas, indicating that the SOWEs could further have impacts on the AABW formation on a longer time scale, which can be investigated by lag correlation analysis and numerical experiments using dyes. Such analysis is beyond the scope of this work and will be conducted in a follow-up study.

5 Conclusions

This study investigated the impacts of strong wind events on sea ice properties and oceanic processes in two Antarctic coastal polynyas based on numerical simulations from the FESOM model. The variations of different sea ice and oceanic variables under SOWEs were quantified and the response time of different properties to the SOWEs was revealed. For both the Prydz Bay and Shackleton polynyas, the SOWEs selected over austral winter were associated with the passage of synoptic- or meso-scale cyclones, which enhanced the offshore wind component in the polynya regions. The offshore sea ice motions and ice production rates in the polynyas increased dramatically and almost instantaneously with the SOWEs and reduced quickly once the SOWEs disappeared. The influence of SOWEs on sea ice concentration persisted for 5–15 days, which may result from the fact that the variability of SIC caused by thermodynamic growth of new ice in the polynyas takes time, and the weaker winds following the SOWEs do not necessarily favor dynamic closing of polynyas. Changes in the
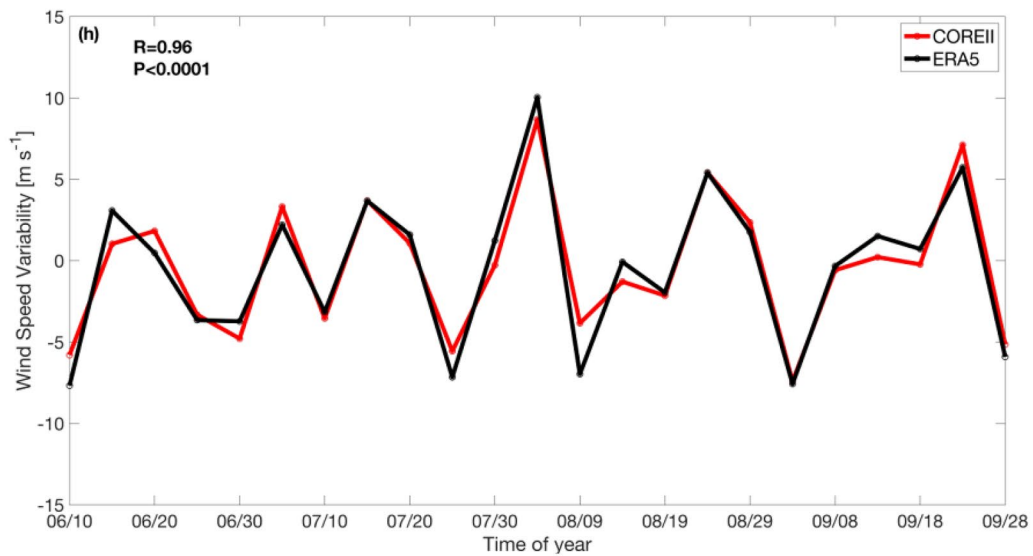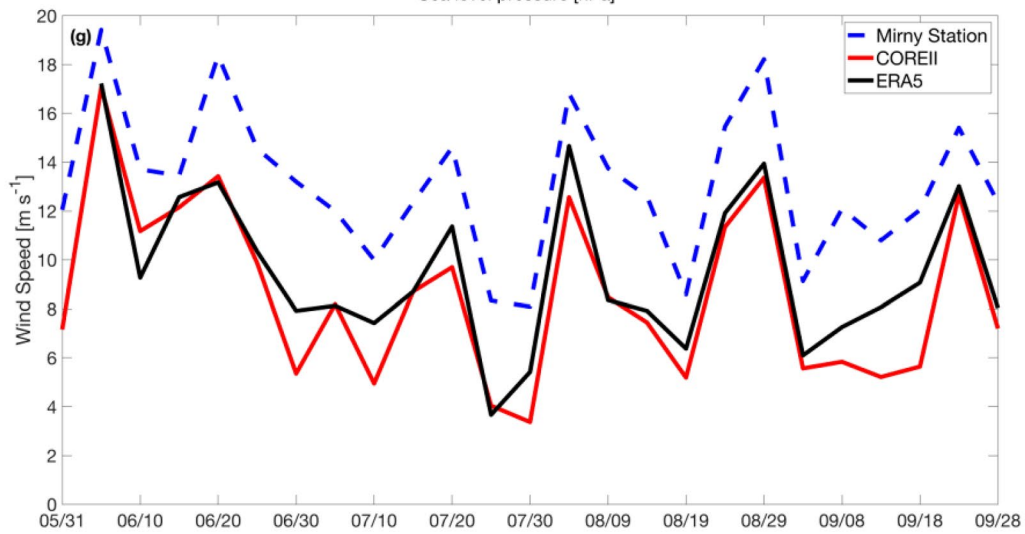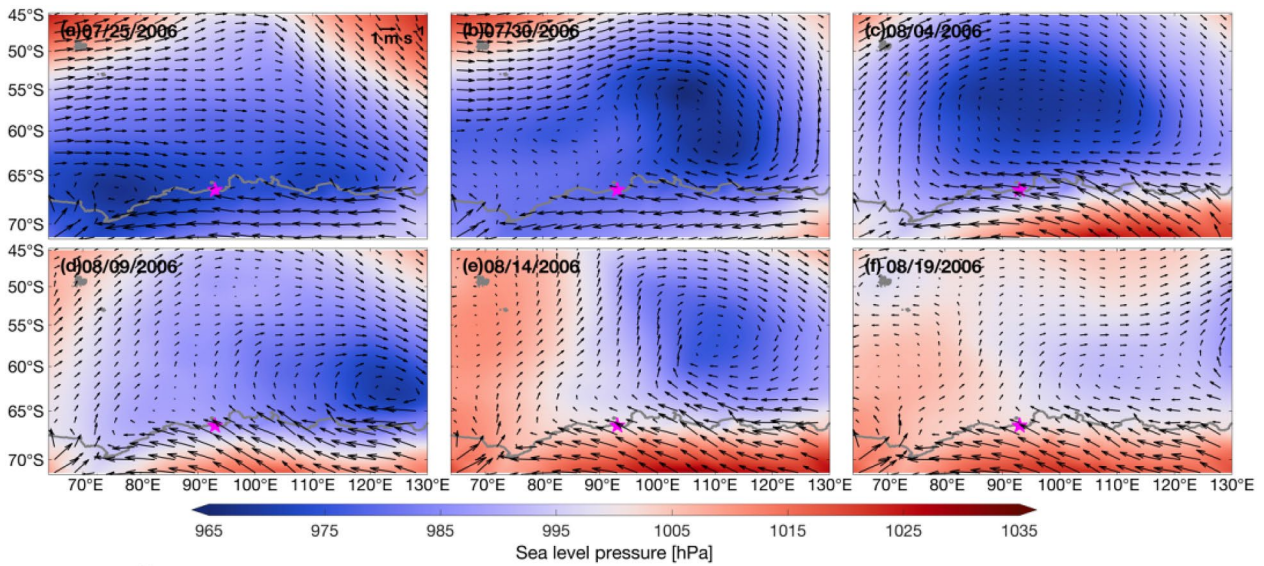
hydrographic properties including the surface salinity and mixed layer depth lagged the SOWEs by about 5–10 days. For both polynyas, the formation of HSSW occurred in the coastal regions at the depth of 200–800 m about 10–15 days post the SOWEs, while there was no significant change in the HSSW characteristics below 800 m. Comparisons of winter mean hydrographic properties in 2 years with different wintertime durations of SOWEs suggest that HSSW features in the deep layers are considerably affected by the SOWE duration in winter.

Realistic representation of sea ice-ocean processes over the Antarctic coastal polynyas are challenging for many of the state-of-the-art coupled models, including the FESOM model, in which a couple of physical processes are missing or not well represented. For instance, the low-resolution CORE-II forcing can induce uncertainties in the coastal wind due to insufficient representation of complex orography, which may further affect the simulation of sea ice production in coastal polynyas. The lack of coupling with the atmosphere could increase the air-sea temperature gradient due to the lack of sensible heat flux transferred from the ocean to the atmosphere, as well as the lack of latent heat flux released into the atmosphere during ice freezing, and colder temperature will result in larger ice production rates. In addition, tides are not included in the FESOM model, but tides could affect sea ice motions (Koentopp et al. 2005) and sea ice production by periodic opening and closing of leads (Luneva et al. 2015). Simultaneously, tides can significantly modulate the export and volume of dense shelf water (Padman et al. 2009; Wang et al. 2013), and favor the inflow of circumpolar deep water onto the continental shelf (Stewart et al. 2018) that can alter stratification in the polynya area and HSSW formation. Finally, the freshwater from ice shelf melting could decrease the sea ice production in polynyas by pumping more circumpolar deep water into the coastal regions (Jourdain et al. 2017; Merino et al. 2018) and suppress the formation of dense shelf water. The impact of ice shelf basal melt on the ocean is largely increased in the presence of tides, and ice shelf basal melt could affect the water mass transport out of polynyas (Huot et al. 2021). The effects
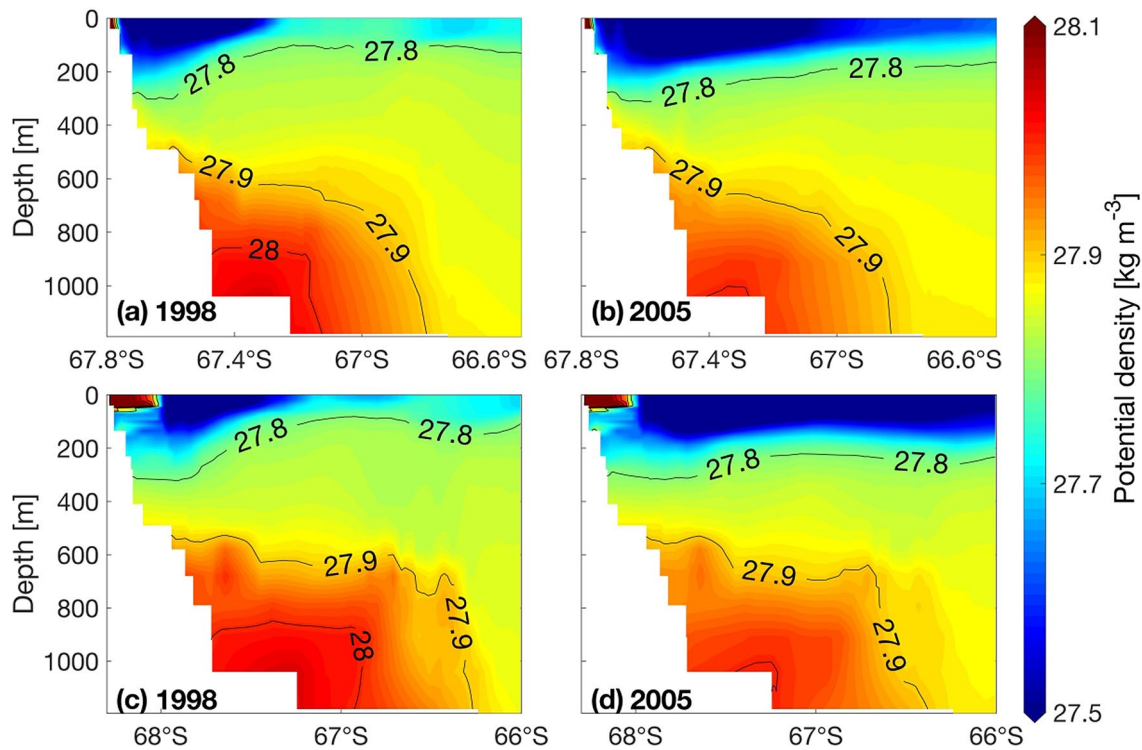
Fig. 19 Vertical transects of potential density **a–b** for the cross-shelf transect indicated by the red line in Fig. 4a and **c–d** for the transect at 80°E in the Prydz Bay Polynya averaged from July to September in **a**, **c** 1998 and **b**, **d** 2005. The black contour lines indicate isopycnals at an interval of 0.1 kg m^{-3}
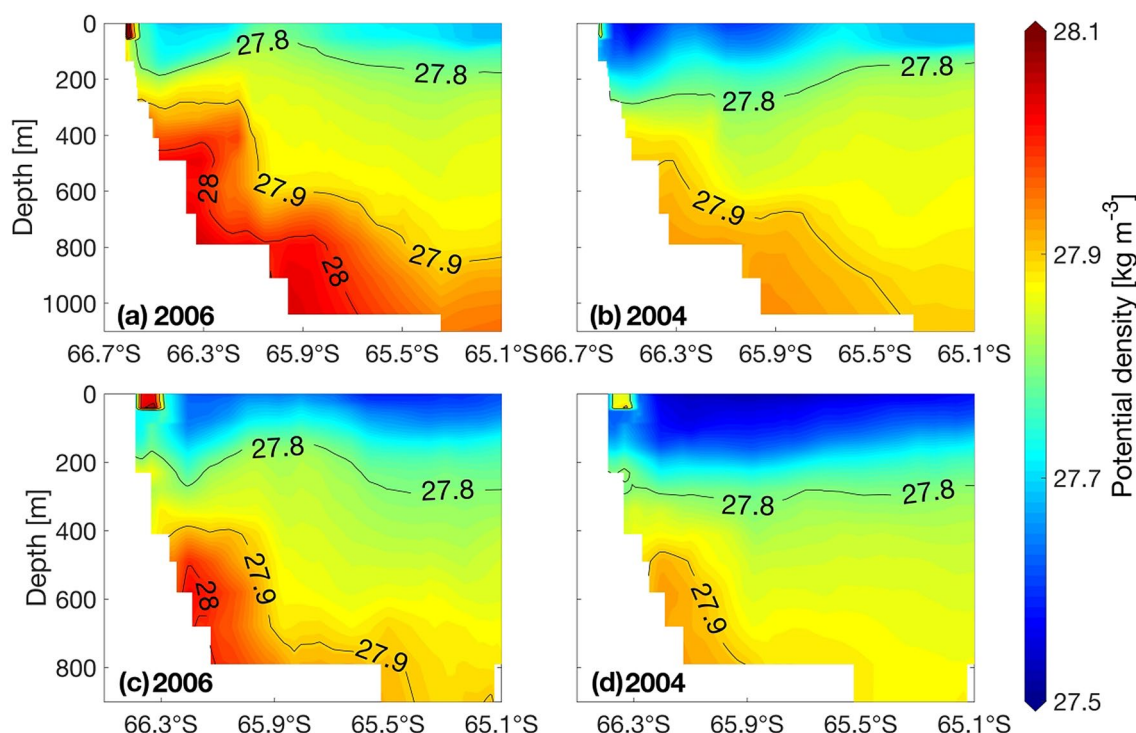
Fig. 20 Vertical transects of potential density for the transect **a**, **b** at 94°E and **c**, **d** at 95°E in Shackleton Polynya averaged from July to September in **a**, **c** 2006 and **b**, **d** 2004. The black contour lines indicate isopycnals at an interval of 0.1 kg m^{-3}

of strong wind events on the tidal and ice-shelf processes as mentioned above can modulate the response of the ice and oceanic response in the coastal polynyas revealed in this study, and these effects should be considered in the future by using models including tidal and ice-shelf modules.

This study employs realistic model simulations to study the response of polynya processes to strong wind events. The atmospheric forcing fields are characterized by consecutive SOWEs, and in such situation it is hard to separate out the response of sea ice and oceanic processes to one single event, as the response time is often longer than the wind event duration time. In the future, idealized numerical experiments can be conducted to reveal the complete responding process of sea ice and in particular, the response of water mass in Antarctic polynyas to the SOWE.

Declarations

Conflict of interest All authors certify that they have NO affiliations with or involvement in any organization or entity with any financial interest (such as honoraria; educational grants; participation in speakers' bureaus; membership, employment, consultancies, stock ownership, or other equity interest; and expert testimony or patent-licensing arrangements), or non-financial interest (such as personal or professional relationships, affiliations, knowledge or beliefs) in the subject matter or materials discussed in this manuscript.

References

Ahrens CD (2000) Meteorology today, 6th edn. Brooks/Cole, Pacific Grove

Arrigo KR, van Dijken G, Long M (2008) Coastal southern ocean: a strong anthropogenic CO_2 sink. Geophys Res Lett. https://doi.org/10.1029/2008gl035624

Barthélemy A, Goosse H, Mathiot P, Fichefet T (2012) Inclusion of a katabatic wind correction in a coarse-resolution global coupled climate model. Ocean Model. https://doi.org/10.1016/j.ocemod.2012.03.002

Bromwich D, Liu Z, Rogers AN, Van Woert ML (1998) Winter atmospheric forcing of the Ross Sea polynya. In: Jacobs SS, Weiss RF (eds) Ocean, ice, and atmosphere: interactions at the Antarctic continental margin, Antarctic research series, vol 75. American Geophysical Union, Washington, pp 101–133

Cheng Z, Pang X, Zhao X, Stein A (2019) Heat flux sources analysis to the ross ice shelf Polynya Ice production time series and the impact of wind forcing. Remote Sens. https://doi.org/10.3390/rs11020188

Comiso JC (2017) Bootstrap sea ice concentrations from Nimbus-7 SMMR and DMSP SSM/I-SSMIS, Version 3 [Indicate subset used]. NASA National Snow and Ice Data Center Distributed Active Archive Center, Boulder. https://doi.org/10.5067/7Q8HCCWS4I0R

Comiso JC, Gordon AL (1998) Interannual variability in summer sea ice minimum, coastal polynyas and bottom water formation in the Weddell Sea American Geophysical Union

Dale ER, McDonald AJ, Coggins JHJ, Rack W (2017) Atmospheric forcing of sea ice anomalies in the Ross Sea Polynya Region. Cryosphere 11:267–280. https://doi.org/10.5194/tc-11-267-2017

Danilov S et al (2015) Finite-element sea ice model (FESIM), version 2. Geosci Model Dev 8:1747–1761. https://doi.org/10.5194/gmd-8-1747-2015

Ding Y, Cheng X, Li X, Shokr M, Yuan J, Yang Q, Hui F (2020) Specific relationship between the surface air temperature and the area of the Terra Nova Bay Polynya, Antarctica. Adv Atmos Sci 37:532–544. https://doi.org/10.1007/s00376-020-9146-2

Dong S, Sprintall J, Gille ST, Talley L (2008) Southern Ocean mixed-layer depth from Argo float profiles. J Geophys Res. https://doi.org/10.1029/2006jc004051

Griffies SM et al (2009) Coordinated ocean-ice reference experiments (COREs). Ocean Model 26:1–46. https://doi.org/10.1016/j.ocemod.2008.08.007

Haid V, Timmermann R (2013) Simulated heat flux and sea ice production at coastal Polynyas in the Southwestern Weddell Sea. J Geophys Res Oceans 118:2640–2652. https://doi.org/10.1002/jgrc.20133

Hoppema M, Anderson LG (2007) Chapter 6 biogeochemistry of polynyas and their role in sequestration of anthropogenic constituents. Polynyas: windows to the world. Elsevier oceanography series. Elsevier, New York, pp 193–221. https://doi.org/10.1016/s0422-9894(06)74006-5

Hunke EC, Dukowicz JK (1997) An elastic-viscous-plastic model for sea ice dynamics. J Phys Oceanogr 20:20

Huot P-V, Fichefet T, Jourdain NC, Mathiot P, Rousset C, Kittel C, Fettweis X (2021) Influence of ocean tides and ice shelves on ocean–ice interactions and dense shelf water formation in the D'Urville Sea. Antarct Ocean Model. https://doi.org/10.1016/j.ocemod.2021.101794

Jourdain NC et al (2017) Ocean circulation and sea-ice thinning induced by melting ice shelves in the Amundsen Sea. J Geophys Res Oceans 122:2550–2573. https://doi.org/10.1002/2016jc012509

Kalnay E et al (1996) The NCEP/NCAR 40-year reanalysis project. Bull Am Meteorol Soc 77:437–472. https://doi.org/10.1175/1520-0477(1996)077%3c0437:Tnyrp%3e2.0.Co;2

Koentopp M, Eisen O, Kottmeier C, Padman L, Lemke P (2005) Influence of tides on sea ice in the Weddell Sea: investigations with a high-resolution dynamic–thermodynamic sea ice model. J Geophys Rese Oceans. https://doi.org/10.1029/2004JC002405

Kusahara K, Williams GD, Tamura T, Massom R, Hasumi H (2017) Dense shelf water spreading from Antarctic coastal polynyas to the deep Southern Ocean: a regional circumpolar model study. J Geophys Res Oceans 122:6238–6253. https://doi.org/10.1002/2017jc012911

Large WG, Yeager SG (2009) The global climatology of an interannually varying air–sea flux data set. Clim Dyn 33:341–364. https://doi.org/10.1007/s00382-008-0441-3

Launiainen J, Vihma T (1994) On the surface heat fluxes in the Weddell Sea Washington DC. Am Geophys Union Geophys Monograph Ser 85:399. https://doi.org/10.1029/GM085p0399

Luneva MV, Aksenov Y, Harle JD, Holt JT (2015) The effects of tides on the water mass mixing and sea ice in the Arctic Ocean. J Geophys Res Oceans 120:6669–6699. https://doi.org/10.1002/2014JC010310

Lutgens FK, Tarbuck EJ (2001) The atmosphere, 8th edn. Prentice Hall, New York

Markus T, Cavalieri DJ (2000) An enhancement of the NASA Team sea ice algorithm. IEEE Trans Geosci Remote Sens 38(3):1387–1398

Massom R, Harris P, Michael K, Potter M (1998) The distribution and formative processes of latent-heat polynyas in East Antarctica.

Ann Glaciol 27:420–426. https://doi.org/10.3189/1998A oG27-1-420-426

Mathiot P, Barnier B, Gallée H, Molines JM, Sommer JL, Juza M, Penduff T (2010) Introducing katabatic winds in global ERA40 fields to simulate their impacts on the Southern Ocean and sea-ice. Ocean Modell 35:146–160. https://doi.org/10.1016/j.ocemod.2010.07.001

Merino N, Jourdain NC, Le Sommer J, Goosse H, Mathiot P, Durand G (2018) Impact of increasing antarctic glacial freshwater release on regional sea-ice cover in the Southern Ocean. Ocean Model 121:76–89. https://doi.org/10.1016/j.ocemod.2017.11.009

Nihashi S, Ohshima KI (2015) Circumpolar mapping of Antarctic coastal polynyas and landfast sea ice: relationship and variability. J Clim 28:3650–3670. https://doi.org/10.1175/jcli-d-14-00369.1

Nihashi S, Ohshima KI, Tamura T (2017) Sea-ice production in antarctic coastal polynyas estimated from AMSR2 data and its validation using AMSR-E and SSM/I-SSMIS data. IEEE J Sel Top Appl Earth Observ Remote Sens 10:3912–3922. https://doi.org/10.1109/jstars.2017.2731995

Ohshima KI et al (2013) Antarctic bottom water production by intense sea-ice formation in the Cape Darnley polynya. Nat Geosci 6:235–240. https://doi.org/10.1038/ngeo1738

Padman L, Howard SL, Orsi AH, Muench RD (2009) Tides of the northwestern Ross Sea and their impact on dense outflows of Antarctic Bottom Water. Deep Sea Res Part II 56:818–834. https://doi.org/10.1016/j.dsr2.2008.10.026

Petrelli P, Bindoff NL, Bergamasco A (2008) The sea ice dynamics of Terra Nova Bay and Ross Ice Shelf Polynyas during a spring and winter simulation. J Geophys Res. https://doi.org/10.1029/2006jc004048

Sein DV, Danilov S, Biastoch A, Durgadoo JV, Sidorenko D, Harig S, Wang Q (2016) Designing variable ocean model resolution based on the observed ocean variability. J Adv Model Earth Syst 8:904–916. https://doi.org/10.1002/2016ms000650

Sein DV et al (2017) Ocean modeling on a mesh with resolution following the local rossby radius. J Adv Model Earth Syst 9:2601–2614. https://doi.org/10.1002/2017ms001099

Smith IJ, Langhorne PJ, Frew RD, Vennell R, Haskell TG (2012) Sea ice growth rates near ice shelves. Cold Reg Sci Technol 83–84:57–70

Steele M, Morley R, Ermold W (2001) PHC: a global ocean hydrography with a high-quality Arctic ocean. J Clim 14:2079–2087

Stewart AL, Klocker A, Menemenlis D (2018) Circum-Antarctic shoreward heat transport derived from an eddy- and tide-resolving simulation. Geophys Res Lett 45:834–845. https://doi.org/10.1002/2017GL075677

Stössel A, Zhang Z, Vihma T (2011) The effect of alternative real-time wind forcing on Southern Ocean sea ice simulations. J Geophys Res. https://doi.org/10.1029/2011jc007328

Tamura T, Ohshima KI, Fraser AD, Williams GD (2016) Sea ice production variability in Antarctic coastal polynyas. J Geophys Res Oceans 121:2967–2979. https://doi.org/10.1002/2015jc011537

Timmermann R et al (2010) A consistent data set of Antarctic ice sheet topography, cavity geometry, and global bathymetry. Earth Syst Sci Data 2:261–273. https://doi.org/10.5194/essd-2-261-2010

Tortell PD, Long MC, Payne CD, Alderkamp A-C, Dutrieux P, Arrigo KR (2012) Spatial distribution of pCO2, ΔO2/Ar and dimethyl-sulfide (DMS) in polynya waters and the sea ice zone of the Amundsen Sea. Antarct Deep Sea Res Part II Top Stud Oceanogr 71–76:77–93. https://doi.org/10.1016/j.dsr2.2012.03.010

Tremblay JE, Smith WO (2007) Chapter 8 primary production and nutrient dynamics in polynyas. Polynyas: windows to the world, Elsevier oceanography series. Elsevier, New York, pp 239–269. https://doi.org/10.1016/s0422-9894(06)74008-9

Turner J, Chenoli SN, Samah A, Marshall G, Phillips T, Orr A (2009) Strong wind events in the Antarctic. J Geophys Res. https://doi.org/10.1029/2008jd011642

Vihma T, Launiainen J, Uotila J (1996) Weddell Sea ice drift: kinematics and wind forcing. J Geophys Res Oceans 101:18279–18296. https://doi.org/10.1029/96jc01441

Vihma T, Tuovinen E, Savijärvi H (2011) Interaction of katabatic winds and near-surface temperatures in the Antarctic. J Geophys Res Atmos. https://doi.org/10.1029/2010jd014917

Wang Q, Danilov S, Hellmer H, Sidorenko D, Schröter J, Jung T (2013) Enhanced cross-shelf exchange by tides in the western Ross Sea. Geophys Res Lett 40:5735–5739. https://doi.org/10.1002/2013gl058207

Wang Q et al (2014) The finite element sea ice-ocean model (FESOM) v1.4.: formulation of an ocean general circulation model. Geosci Model Dev 7:663–693. https://doi.org/10.5194/gmd-7-663-2014

Weber NJ, Lazzara MA, Keller LM, Cassano JJ (2016) The extreme wind events in the Ross Island Region of Antarctica. Weather Forecast 31:985–1000. https://doi.org/10.1175/waf-d-15-0125.1

Whitworth T, Orsi AH, Kim SJ, Nowlin Jr WD, Locarnini RA (2013) Water masses and mixing near the antarctic slope front. In: Ocean, ice, and atmosphere: interactions at the Antarctic Continental Margin, pp 1–27. https://doi.org/10.1029/AR075p0001

Yoon S-T et al (2020) Variability in high-salinity shelf water production in the Terra Nova Bay polynya. Antarct Ocean Sci 16:373–388. https://doi.org/10.5194/os-16-373-2020

Zhang Z, Vihma T, Stössel A, Uotila P (2015) The role of wind forcing from operational analyses for the model representation of Antarctic coastal sea ice. Ocean Model 94:95–111. https://doi.org/10.1016/j.ocemod.2015.07.019

Zubov NN (1945) Arctic ice. US Navy Electronics Laboratory, New York, p 491